Thunderstorm characteristics favouring downward and upward lightning to wind turbines

Nicolau Pineda, Joan Montanyà, Albert Salvador, Oscar A. van der Velde, Jesús A. López

PII: S0169-8095(18)30073-5
DOI: doi:10.1016/j.atmosres.2018.07.012
Reference: ATMOS 4317

To appear in: *Atmospheric Research*

Received date: 16 January 2018
Revised date: 10 July 2018
Accepted date: 10 July 2018

Please cite this article as: Nicolau Pineda, Joan Montanyà, Albert Salvador, Oscar A. van der Velde, Jesús A. López , Thunderstorm characteristics favouring downward and upward lightning to wind turbines. Atmos (2018), doi:10.1016/j.atmosres.2018.07.012

THUNDERSTORM CHARACTERISTICS FAVOURING DOWNWARD AND UPWARD LIGHTNING TO WIND TURBINES

Nicolau Pineda [a,b], Joan Montanyà [a], Albert Salvador [a,b], Oscar A. van der Velde [a], Jesús A. López [a]

[a] Lightning Research Group, Technical University of Catalonia, Carrer Colom 1, 08222 Terrassa, Spain

[b] Meteorological Service of Catalonia, Carrer Berlín 38-46, 08029 Barcelona, Spain

Contact: npineda@meteo.cat

ABSTRACT

Meteorological conditions and thunderstorm characteristics related to lightning threats to wind turbines are discussed in this paper. Due to the rotating blades, wind turbines may be regarded peculiar tall objects, more susceptible to lightning strikes than other tall man-made structures. In the present study, Lightning Mapping Array and weather radar observations allowed to draw a clear picture of the thunderstorm characteristics leading to lightning strokes to wind turbines, in a coastal area of the Mediterranean basin. Results showed that lightning threats to wind turbines tend to occur during transitional periods (spring and autumn), although the main thunderstorm activity concentrates in the warm summer months. Thunderstorms with downward strokes to wind turbines presented particular features, like a limited vertical development and a dominant lower positive charge layer. Downward cloud-to-ground strokes hitting wind turbines were mainly of negative polarity and with peak currents above the average. On the other hand, conditions for self-initiated upwards from wind turbines resemble those reported in Japan and the U.S winter thunderstorms, with low-cloud based large electrified stratiform regions. These particular conditions, leading to lightning threats to wind turbines, should be properly included in lightning protection standards.

KEY WORDS: lightning mapping array, thunderstorm charge structure, downward and upward lightning, wind turbines

1. INTRODUCTION

The observations of lightning strokes to tall objects have been extensively reported in the literature (e.g. McEachron, 1939; Berger, 1967; Eriksson, 1978). A summary of the research efforts on this subject can be found in Rakov and Uman (2003). Interest in lightning to tall structures has grown in recent years, in particular due to the rapid expansion of wind energy globally (e.g. Rachidi et al., 2008; Foley et al., 2012).

Structures of limited height (below 100 m) will suffer from downward strikes whereas tall structures like wind turbines (hereafter, WT) are more prone to initiate upward lightning (e.g. Rachidi et al., 2008; Zhou et al., 2010). High towers (>100 m height) are exposed to strong local electric fields under thunderclouds, being prone to initiate upward propagating leaders (Berger, 1967). Besides, local topography plays a role on the effective height of the structure. Towers on mountain tops are said to have an effective height that is considerably larger than the physical height of the tower (e.g. Risk 1990; Rachidi et al., 2008; Zhou et al., 2010). The concept of effective height is used to account for the additional field distortion (enhancement)

due to the presence of the mountain on which the structure is located (e.g. Pierce, 1971; Eriksson, 1978; Risk, 1994; Zhou et al., 2010).

In addition, rotating blades make WT peculiar tall objects (almost 40% of the total turbine height is in rotation). In this regard, a growing number of studies speculate whether a rotating WT is more susceptible to lightning strikes than stationary turbines (e.g., Rachidi et al., 2008; Wang et al., 2008; Radicevic et al., 2012; Wang and Takagi, 2012; Montanyà et al., 2014). According to Montanyà et al. (2014) the effect of rotation induces an electric field growth rate, necessary for the initiation of stable leaders.

All in all, tall structures like multi-megawatt WT have a higher probability of being struck by lightning, compared to their surroundings (e.g. Rachidi et al., 2008; Wang and Takagi, 2012). Indeed, lightning is one of the major causes of severe damage to WT and add a significant cost to their operation and maintenance (e.g. Braam et al., 2002; Minowa et al., 2006; Yasuda et al., 2012; Candela et al., 2014).

1.1. Type of lightning to tall structures

Lightning strikes can be divided into several categories, where the ones relevant to WT mainly concern lightning polarity and the direction of initiation. Downward lightning occurs mainly under deep convection (e.g. warm-season thunderstorms) and the threat to WT calculated in relation to the regional lightning density (Ng). Downward discharges are predominantly of negative polarity, in correspondence with lightning climatology (Rivas-Soriano et al., 2005; Pineda et al., 2011; Poelman et al., 2016).

As mentioned previously, tall structures above a certain height are prone to initiate upward lightning (UL). Leaders may originate from WT due to locally strong electric fields (self-initiated upward lightning, SIUL) or may be triggered by prior lightning discharges in the vicinity, which can provide the necessary electric fields for the inception of an upward leader (lightning-triggered upward lightning, LTUL). Regarding WT, Wang and Takagi (2012) noted that self-initiation occurred more frequently with higher observed wind speeds (or a rotating windmill) compared with LTUL. It should be added here that upward propagating leaders not followed by return stroke sequences can go unnoticed by conventional Lightning Location Systems (LLS), and therefore the number of upward leaders from WT will be underestimated (e.g. March, 2017).

Despite the modest occurrence of winter lightning, compared to lightning activity associated to deep convection, winter thunderstorms can produce very energetic lightning events (Zhou et al., 2012a; 2012b), and a large amount of damage to sensitive tall structures such as WT (e.g. Shindo et al., 2012; Wang and Takagi, 2012; Yokoyama, 2013; Honjo, 2015). The underlying reason is the low altitude of the cloud charge, as well as the reduced or even absent lower positive charge region (Murphy et al., 1996; Montanyà et al., 2007; Nag and Rakov, 2009; Williams, 2018). Although the highest winter lightning activity is reported in Japan, Montanyà et al. (2016a) identified other areas prone to winter lightning such as parts of the Mediterranean basin, the eastern coast of the US or in the Southern Hemisphere, Uruguay and its surroundings. For example, Levin et al. (1996), Yair et al. (1998) and Altaratz et al. (1999) have reviewed the meteorological conditions favouring lightning in the eastern Mediterranean. There, winter lightning activity concentrates between December and February. Thunderclouds develop at the cold front or, within the cold air mass, just immediately after passing through the "Cyprus lows" (Altaratz et al., 2001). This type of storm is very similar to winter thunderstorms in western Japan (Michimoto, 1991; 1993), and is different from the summertime, continental, mesoscale convective system type thunderclouds.

1.2. Lightning risk assessment

Current lightning protection standards for WT (e.g. IEC 61400-24, 2010) rely on three main parameters: (i) the lightning density (Ng) of the region where the wind farm is to be installed; (ii) the height of the wind turbine itself and (iii) the environmental factor (Cd). Downward lightning is the most frequent type of lightning and its incidence on a particular wind farm is related to the local Ng. Conversely, UL is only considered in the standard within the environmental factor, among other factors like the complexity of local terrain and the height above sea level. According to different authors (e.g. Rachidi et al., 2008; March 2017) the majority of the strikes to modern turbines are expected to come from UL, and therefore a more realistic approach to calculate its contribution is suggested (e.g. Chan et al., 2018). A proposal on how to account for UL in protection standards is beyond the scope of this paper, but the aforementioned issues emphasise the importance of expanding the knowledge on this topic.

1.3. Objectives

There has been very little study of the in-cloud components of UL from man-made structures. In recent years, the use of high resolution lightning mapping systems and high-speed video have provided relevant information about lightning occurrence on WT. Observations of lightning initiated by WT with a Lightning Mapping Array (LMA) system (Van der Velde et al., 2011; Schultz et al., 2011; Montanyà et al., 2014; Wang et al. 2017), as well as of direct impacts from downward strokes (Montanyà et al., 2016b) have been recently presented. Bearing in mind the growing concern on the lightning impact on the wind power sector as the wind farm deployment grows around the globe, it is of interest to analyse the meteorological context that favours lightning to/from WT. In particular, our objective in the present study was to identify the characteristics and common features of the thunderstorms that produced flashes striking WT in a coastal area of the western Mediterranean basin. To this end, the analysis mainly relied on LMA, weather radar volumetric data and temperature vertical profiles, to characterise thunderstorms that pose a threat to WT, with special emphasis on the vertical charge structure.

The area of study (hereafter, AoS) is a hilly area in south Catalonia, near the river Ebre's Delta, not far from the coast on the western Mediterranean Sea (Fig. 1). Wind farms have been progressively deployed in the AoS since 1995. Roughly speaking, wind farms consist of 25 to 50 small WT (40-80 m height), with a baseline ranging from 150 to 250 m and produce from 5 to 50 MW. The AoS is an area largely covered by meteorological observation systems, as it has been designed to cover the post launch Cal/Val field campaign of the ASIM project (Neubert et al., 2006).

The organization of the paper is as follows: Section 2 describes the instrumentation and analysis technique; Section 3 collects the results; Section 4 deals with the discussion of the results and finally section 5 presents the concluding remarks.

2. INSTRUMENTATION AND ANALYSIS TECHNIQUES

2.1. Intra-cloud lightning

Intra-cloud (IC) lightning was measured with a LMA (Rison et al., 1999; Thomas et al., 2004) deployed in the Ebre's Delta during the summer of 2011 (Fig. 1). The LMA system detects lightning radio emissions in the very high frequency range (VHF, 60–66 MHz) and locates them in three dimensions by a time-of-arrival (TOA) technique. Each station samples, over 80 μs intervals, the maximum signal amplitude and its GPS-

derived precise time, allowing to locate 2000 to 3000 sources per second coming from lightning channels inside the cloud. The accuracy of the mapped source locations is expected to be within 10 m in the horizontal dimension, 30 m in the vertical dimension and 40 ns in time (Thomas et al., 2004). This level of accuracy allows identifying the upward leaders associated with a WT.

The so called Ebre Lightning Mapping Array (ELMA) is operated by the Lightning Research Group of the Technical University of Catalonia (http://lrg.upc.edu/en). The initial six-station ELMA was expanded to 11 stations during 2012, enlarging the area of coverage. Details on the ELMA can be found in Van der Velde and Montanyà (2013).

2.2. Cloud to ground lightning

Cloud-to-ground (CG) data is needed to complement the LMA, since the LMA only detects the cloud phase of lightning. CG stroke information used in the current study was obtained from the LLS operated by the Meteorological Service of Catalonia (SMC), composed by four VAISALA LS8000 stations covering the region of Catalonia (NE Iberian Peninsula) including the AoS. CG return strokes are detected by a low frequency (LF) sensor and located using a combination of TOA and Magnetic Direction Finding (MDF) technique (Cummins and Murphy, 2009). Throughout the years of operation, the SMC-LLS performance has been experimentally evaluated by means of electromagnetic field measurements and video recordings of natural lightning in successive campaigns (Montanyà et al., 2006; 2012; Pineda and Montanyà, 2009). The analysis of the 2013-campaign (Montanyà, 2014) establishes a CG flash detection efficiency for the SMC-LLS around 80–85%.

Additionally, CG data from the European LINET network was available for the analysed events. LINET employs TOA to detect CG lightning strokes in the very low frequency range Betz et al. (2009a). LINET offers a location accuracy reaching an average value of around ~150 m, as verified by CG strokes to towers of known position (Betz et al. 2009a). More details about the LINET system can be found in Betz et al. (2009b).

2.3. Weather Radar

In this work, we also took advantage of weather radar products. The SMC operates a weather radar network in the Catalonia region, with "La Miranda" radar (N 41° 05′ 30.24″ E 0° 51′ 48.58″; 950 m above MSL) located at 40–50 km of the AoS (Fig. 1). The SMC radars operate in C-band (5.600 to 5.650 MHz) and are Doppler type. Polar volumes (radar reflectivity and radial velocity) are acquired every 6 min. Further technical details of the SMC weather radars and network characteristics can be found in Bech et al. (2004) and Argemí et al. (2014).

Since the introduction of weather radar, many studies have dealt with the necessary conditions for the initiation of lightning (e.g. Workman and Reynolds, 1949; Reynolds and Brook, 1956; Larsen and Stansbury, 1974; Dye et al. 1989; Buechler and Goodman, 1990; Hondl and Eilts, 1994). All in all, the onset of significant electrification is associated with a rapid vertical development of convection, which allows the presence of precipitation in the mixed phase region (i.e., the presence of small ice crystals and super-cooled cloud water) above the height of the –10°C isotherm. Therefore, the appearance of a 30–40 dBZ or greater radar echo at heights above the –10°C isotherm indicates the presence of a large enough quantity of hydrometeors in the mixed phase region for electrical charging, and ultimately, lightning.

To account for the thunderstorm vertical development, we worked with the radar echo top product, with 12 and 35 dBZ thresholds (that is, the maximum height reached by the 12/35 dBZ reflectivity echoes). Besides, constant-altitude plan position indicator (CAPPI) at 1000 m AGL images, were used to analyse the storm morphology.

2.4. Sounding vertical profiles

Reviews of charge structure (e.g. Khrehbiel, 1986; Williams, 1989) illustrate a relationship between the height of electrical charge centres and the temperature profile. In this regard, the heights of the representative environmental temperature values selected were obtained from the Barcelona radiosonde data (Abellán et al., 2011). The Barcelona station (N 41º 23' 4.08" E 2º 7' 3.36") takes part on the Global Telecommunications Service (GTS) observations from 2008, with the code 08190.

Relying on the graupel–ice mechanism conceptual model to explain cloud electrification (e.g. Takahashi, 1978; MacGorman and Rust, 1998), the environmental temperatures selected in this study were –10°C and –40°C, aiming to delimit the mixed-phase cloud region, where the main negative charge region resides (MacGorman and Rust, 1998). In fact, many studies have reported a strong correlation between lightning initiation and radar echoes at –10°C to –20°C levels (e.g. Krehbiel et al. 1984; Buechler and Goodman, 1990; Gremillion and Orville, 1999; Vincent et al., 2003; Yeung et al., 2007). Krehbiel et al. (1984) has noted that this main negative charge region remains at fairly constant altitudes as the storm evolves. Moreover, Tomine et al. (1986) and Michimoto (1991) have stated that these environmental temperatures also apply to winter storms, despite taking place at rather low altitudes.

On the other hand, two instability indices derived from the Barcelona sounding were used to briefly characterise the environment of the analysed thunderstorms: the CAPE (Convective Available Potential Energy, Wallace and Hobbs, 1973), a common metric for the energy available in the environment for thunderstorm growth; and the Lifting Condensation Level (LCL), used to estimate boundary layer cloud heights (e.g., Stackpole, 1967).

2.5. Case study selection

Episodes with lightning flashes involving WT in the AoS were primarily identified by means of LINET CG data. Since clusters of CG are often observed around tall structures (e.g. Betz et al., 2004; Diendorfer et al 2014, Nag et al 2015), the area with wind farms within the LMA coverage was systematically monitored, looking for clusters of strokes in a buffer of 150 m around WT. Data from this first selection was manually inspected using LMA data, searching for leaders ending or starting on WT. This exercise resulted in 5 case studies. Besides, two summer thunderstorm episodes are included in the analysis, in order to have a reference on the typical warm-season vertical charge structure for comparison.

2.6. Analysis technique

The analysis of the evolution of the vertical structure of the storm relied mainly on the evolution of the LMA source density, two radar echo top products (12 and 35 dBZ) and temperature vertical profiles (–10°C and –40°C). Besides, the vertical charge structure was inferred from the LMA observations for the periods when lightning to/from WT occurred. In particular, we used the method developed by van der Velde and Montanyà (2013), which uses a time-distance-altitude projection to identify the polarity of each IC leader process from the inferred velocity of lightning channels. The LMA predominantly locates sources coming from negative leaders moving through regions of positively charged cloud particles, with propagation speeds

of $1–2·10^5$ ms^{-1}. Weaker sources from positive leader traces inside the negative charge region are often detected as well, caused generally by recoil leaders (e.g., Mazur, 2002; van der Velde and Montanyà, 2013). Compared to negative leaders, the propagation speed of positive channels is almost an order of magnitude lower, with velocities around $2–3·10^4$ ms^{-1} (e.g. Mazur et al., 1998; Shao and Krehbiel, 1996). The majority of these sources typically cluster over a shallow range of altitude, creating regions of net positive and negative charge. LMA observations have also shown that the lightning discharge tend to initiate in-between these opposite charge layers (van der Velde and Montanyà, 2013).

Finally, to account for the horizontal dimensions of the storm system, storm morphology analysis was carried out using the classifications by Parker and Johnson (2000) and Duda and Gallus (2010). All systems were classified using visual inspection of radar CAPPI sequences.

3 RESULTS

The case studies with lightning strokes to WT are summarized in Table 1, which includes both downward and upward lightning events. The selection of case studies includes also includes two summer thunderstorm episodes, to be used as a reference for typical warm season thunderstorms in the analysis and discussion of the charge structure.

3.1. Lightning activity in the region of interest

The first thing to stress about Table 1 is that the episodes involving lightning strokes to WT correspond usually to months with low lightning activity in the AoS, such as April and November. Therefore, before the case overview, lightning patterns throughout the year in the AoS were analysed, using data from the SMC-LLS (12–year period, 2005–2016). The average CG flash density in the AoS is of 2.8 CG flashes km^2 $year^{-1}$, 0.8 above the average density of the whole Catalonia. On the one hand, nearly 87% of the annual CG flashes occur between June and October, with a peak at the end of summer (24% in August and 33% in September). Conversely, months from November to April account for only 9% of the observed lightning activity. Indeed, the seasonal cycle in the AoS is driven by two main factors: the solar heating which peaks in summer and favours the onset of convective storms, and the proximity to the Mediterranean Sea conditioning the autumn and winter activity. From the late summer on, lightning activity moves gradually to the coast and offshore, where the activity is dominant in autumn. This change is related to the average land/sea temperature difference, the average sea surface temperature being warmer during autumn compared to land (Kotroni and Lagouvardos, 2016; Galanaki et al., 2018).

3.2. Typical summer thunderstorms. Case overview

1st JULY 2014

On that day, convective indices presented moderate conditions of instability (see Table 1). Convection started to develop in the mountainous region west of the Ebre's Delta, traveling to the Northeast afterwards. The initial cells began to cluster in a line, oriented in the direction of the predominant SW-NE flow. Over time, the flow rotated to a West-East pattern. New growing cells kept clustering but in a less organized manner. The cluster of cells crossed the AoS between 17:00 and 18:00 UTC and promptly decayed soon after. Fig. 2 shows the evolution of the vertical structure of the storm occurring in the AoS. Thunderstorms in this episode began to grow rapidly around 11:00 UTC, and continued intensifying until 15:00 UTC, as indicated by increases both in the density of VHF sources. The seesaw trend of the TOP–35 in the following

hours suggests a sequential development of pulse-type convection. High IC activity was reported by the LMA as the TOP–35 remained around the –40°C. The abrupt decay of the TOP–35 by 18:30 UTC led to the termination of the lightning activity. It is worth noticing the increase in the CG lightning flash rate (hereafter LFR) on the latest hours, as the VHF burst density showed activity in the lower positive layer (16:30 – 18:00 UTC approx.).

2nd AUGUST 2014

Convection initiated around 11:00 UTC with diverse cells that progressively clustered SW of the Delta, to finally form a non-linear convective system with a large area of reflectivity above 45 dBZ (CAPPI 1km 13:00 UTC) in what looks like the period of maximum development. After that, while moving to the Ebre's Delta from West to East, the complex split into different cells, to finally dissipate around 14:00 UTC. In the meantime, new cells appeared in the radar coverage coming from SW, this time showing a leading stratiform pattern. Subsequent cells continued in the same SW-NE flow over the Delta. The 35–dBZ echo tops (Fig. 3), growing rapidly to reach first the –10°C (4.5 km AMSL approx.) and shortly after the –40°C (9 km AMSL approx.), spanning the mixed-phase region, suggested the presence of graupel and an environment conductive to active charge separation. The LMA density bursted shortly after, showing a high activity between 12:00 and 14:00 UTC, related to negative channels at heights between 9–11 km ASML. Negative channels in the lower layer also became apparent from 12:00 to 13:00 UTC, coinciding with the period of maximum LFR (15 CG min^{-1}). Between 13:00 and 14:00 UTC the TOP–35 almost lost half of its height, and so did the VHF source density and the CG activity. In the following hours the TOP–35 stayed around the -10°C with a moderate lightning activity until a rapid decline around 20:00 UTC.

3.3. Case studies involving lightning to wind-turbines

The cases listed in Table 1, involving lightning strokes to WT, showed modestly unstable environments with 400 J kg^{-1} of CAPE at most, –10°C levels below 4500m AMSL, nearly saturated vertical profiles and the tropopause at around 10–11 km AMSL or lower. Accordingly, the resulting storm systems were not particularly vigorous. Weather radar sequences showed that thunderstorms favouring lightning strokes to WT did not have any particular precipitation configuration. Besides, they all showed a weak LFR, with lightning to WT occurring around the maximum LFR period.

20th NOVEMBER 2011

For this episode, radar imagery showed a stationary thunderstorm system with a parallel-stratiform precipitation configuration, moving SE-NW, with weak convective cells at its southernmost end. The VHF source density (Fig. 4) shows two periods of maximum activity, the first around 04:30 UTC and the second at 07:30 UTC, with a strong lower positive layer at 3–4 km ASML and a weaker upper positive layer between 7 and 9 km ASML. These two periods of maximum activity are delimited by TOP–35 above the –10°C height, and the moments of maximum LFR (7–8 CG min^{-1}) are collocated with the maximum TOP–35 heights. Downward lightning to WT (04:29, 04:37, 04:39, 04:45 UTC) were observed during the first period of maximum activity. At that time, 1-km CAPPI imagery showed a rainfall field extension (>12 dBZ) at that time of about 100 x 40 km. Another series of downwards to WT was observed between 06:55 and 07:15 UTC (06:55, 06:57, 06:58, 07:11, 07:15 UTC), coinciding with high VHF source densities in the low charge layer.

As an example, the LMA plot of the 04:37 UTC flash is shown in Fig. 5. The flash started immediately above a wind turbine with a fast negative downward leader originated at around 3 km altitude, producing two CG strokes to a WT. The first CG stroke produced a current of –98 kA, the second stroke was of –7 kA

and occurred 23 ms after. The flash had a low altitude positive leader development with negative leader activity above. No leader activity was observed above 6 km during this lightning event. The plain view panel shows radial channels spreading simultaneously in various directions, all starting from the lightning initiation region. Regarding to the precipitation structure, Fig. 6 shows the 04:39 UTC flash in combination with the radar reflectivity. Similar to the 04:37 UTC flash (Fig.5), this flash also started on the perimeter of a convective core, with a downward channel right after the breakdown, and cloud channels spreading radially to the stratiform precipitation region after the CG return stroke. The second series of lightning to WT had a similar pattern, with the CG flashes to WT starting in the vicinity of convective cores, showing first CG strokes followed afterwards by cloud channels spreading away.

3rd APRIL 2012

At the time of the first downward flashes to WT (18:38, 18:44 UTC), the north-eastward moving thunderstorms looked like a trailing-stratiform system with embedded weak convective cores above the AoS. Two periods of IC activity were observed above the AoS, the first one starting around 13:00 UTC when the TOP–35 reached the –40°C height (the evolution is not shown). After a short period of inactivity, activity restarted between 18:00 and 19:30 UTC approx. The sequence of the LMA source density indicates a progressive decrease in the height of the low charge layer. The downward stroke to a WT occurred during this later period.

Fig. 7 shows the LMA detection of the downward stroke that impacted a WT during this episode. Note that the leader activity stayed below 6 km a with remarkable positive leader development. A negative leader to ground started at the beginning of the flash and ended with a –18 kA stroke to a turbine located on one of the wind farms in the AoS (≈640 m AMSL). According to the radar imagery analysis (not shown), in this case the leader initiated in the rear edge of a convective cell and hit a turbine which was under the same cell at that moment. Compared to precedent case, maximum reflectivity was slightly higher, but the vertical development was similar, with the Top–35 reaching 6.0 to 7.0 km.

17th NOVEMBER 2012

Around 11:00 UTC, a broken line of cells crossed the AoS South to North, progressively transforming into a parallel stratiform precipitation structure. From 13:00 UTC some of the cores intensified to reach 50 dBZ. Around 17:30 UTC the storm intensity decreased still, the system remained active and intensified again by 22:00 UTC. However, by that time the main cells were leaving the area of coverage of the LMA and were not well represented in Fig.8. VHF source density detected by the LMA shows a bimodal distribution with maximums at 3–4 km and 6–7 km height (similar to the precedent cases). A downward lightning flash to a WT was identified at 17:34 UTC (see Fig. 9). This case corresponds to a complex flash originated about 50 km away from the WT. Before striking the turbine, an intense +CG stroke (+52 kA) triggered a sprite (see van der Velde et al. 2014). After the long negative leader had passed near the WT, positive breakdown occurred and suddenly a negative leader was directed towards a WT, producing 9 strokes. The leader sequence suggests that the first leader development related to the intense +CG flash initiated a new leader breakdown in the wind turbine area. Radar reflectivity in Fig 9 helps locating the negative leader which starts at the border of a convective cell with maximum reflectivity around 45 dBZ. The cloud channel crossed a stratiform area with lower reflectivity, to finally reach a WT which was close to a smaller convective core.

16th NOVEMBER 2013

On that day, radar imagery showed a leading stratiform precipitation structure, with a large area of moderate reflectivity reaching the AoS around 05:30 UTC. Lightning activity in the AoS was mainly related to embedded convection cores that formed offshore. Ground temperature was about 8°C with a cold air mass from the North and a flow from the Mediterranean due to a low. In this case, the storm was close to the threshold for being considered a winter thunderstorm according to Montanyà et al (2016a) criteria. The evolution of the vertical structure of the storms occurring in the AoS for this episode (not shown) limits the presence of lightning to a narrow timespan of one hour between 08:15 and 09:15 UTC approximately. This is the only period where the TOP–35 was above the –10°C level (3,100 m AMSL). It is during this period that the upward flashes were detected by the LMA (08:13, 08:37, 08:41 UTC). Fig. 10 reveals pulses related to an upward positive leader, starting close to the ground. After 400 ms approx., a very well resolved negative leader rapidly accelerated upwards into a layer of positive charge. The right panel of Fig. 10 shows leader speeds (van der Velde and Montanyà 2013). In this case, the likely source of the UL was a WT. The flash grew to a size of 65 by 40 km. There seem to be two other upward leaders in the figure (435.6 s and 435.85 s), but not as well resolved by the LMA as the first one.

18TH JANUARY 2014

In the AoS, thunderstorms occurring in winter months like the present case study are usually associated with fronts moving northward along the Spanish east coast, or with Mediterranean humid, unstable air lifted over the elevated terrain near the coast. According to the radar sequence of that day (not shown), around 05:00 UTC some weak cells started crossing the AoS, South to North. From 06:30 UTC, some organisation became apparent, which can be described as a weak leading stratiform precipitation system. It produced lightning between 08:00 and 10:00 UTC aprox. During that period, the evolution of the vertical structure of the storm (not shown) depicted negative channels at two different layers, the upper corresponding to positive charge level between 7 to 9 km, with the low positive layer around 4–5 km. Four downward CG strokes to WT were observed between 08:40 and 09:37 UTC. As an example, Figure 11 presents the flash to a WT that occurred at 08:40:18 UTC. Like in the 20th November 2011 episode (Fig.6), the flash initiated in the vicinity of a convective core. The LMA depicts a flash starting at 3 km height with a stepped leader that produced three CG strokes to WT (–36, –13, –9 kA). However, this time, the following cloud channels stayed around the core and did not spread to the stratiform region.

Besides, a lightning triggered upward flash was reported at 09:00 by the ELMA (see Fig 12) Although the leader trail was not as well-defined as in the upward flashes detected on the 16th November 2013, it seemed to initiate from a WT. The flash started with a negative CG, followed by cloud positive leader at 4–5 km height. Half a second after the beginning of the event, negative strokes reported by LINET were followed by negative leaders, spreading at 8–9 km height, before the negative leader from a WT accelerated upwards to reach the negative layer at 6–7 km height. No other strokes where recorded by LINET after the upward leader.

3.4. Inferred charge structure

As seen throughout this study, the LMA system depicts the height of the localised VHF sources, predominantly coming from negative leaders moving through positively charged regions. Therefore, the relative density of sources can be used to infer the charge structure inside the thunderstorm cells. Indeed, the majority of these sources typically cluster over a shallow range of altitude, as shown in the previous evolution figures. However, we do not intend here to do a complete characterization of thunderstorms

charge structure. Instead, our focus lies on the period with lightning activity concerning WT. Hence, vertical profiles of the charge layer structure have been inferred for the periods in which lightning to/from WT occurred (Fig. 13). While the relative density of LMA sources helps locating the charge layer altitudes, the dominant polarity on each layer was confirmed through the inferred velocity of lightning channels, using the aforementioned method by van der Velde and Montanyà (2013).

As expected, typical summer storms display the basic tripole structure (Williams, 1989, 2001). After a rapid vertical growth (Fig 2, 3) a dipole developed, the upper positive charge layer reaching 10–11 km height (–40ºC). The negative charge region below, related to the mixed phase region (e.g. Williams et al 1991), is located between the 5 and 8 km height (–10ºC to –25°C). Figs. 2 and 3 also show, at certain stages, the development of a lower positive charge layer, constituting the classical tripole structure.

Interestingly, apart from the 16th November episode, all the other cases analysed showed the same basic tripole structure, the difference being the vertical development they reached. Whereas the upper positive layer reached the 10 km AMSL in the warm season episodes, the cases with downward lightning to WT, only reached 8–9 km height. On the other hand, it is worth noticing that the lower charge positive region is closer to the surface in all the lightning to WT related episodes. Besides, higher LMA source densities were found on the upper positive layer in the summer reference cases, while LMA source activity dominates in the lowest positive charge layer in the WT related cases.

4. DISCUSSION

4.1. Charge Structure

Results showed charge structures that can be compatible with the tripole produced by the non-inductive charge mechanism (NIC, e.g. Takahashi, 1978; Williams, 1989; Saunders et al., 2006). The LMA inferred charge layers shown in Fig 13 suggest three different types of structure. Firstly, the LMA source density in the warm-season convection episodes (Figs. 2 and 3) shows the maximum activity concentrated in the upper positive charge layer. Deep-convection results in elevated charge structures, with large total LFR but low ground LFR. The CG LFR increases only when a low charge layer is apparent (see Figs. 2 and 3).

Secondly, spring and autumn episodes (e.g. 3rd April, 17th Nov., 20th Nov, Figs. 4 and 8), also having a tripole structure, share another common feature: the lower positive charge layer is the dominant (contrary to warm-season convection where the upper level dominates). This particularity will result in an enhancement of the electric field at the bottom of the negative charge region, providing the means to discharges to propagate to ground as CG flashes (e.g., Jacobson and Krider 1976, Williams 2001, Marshall and Stolzenburg 2002, Pawar and Kamra 2004). Early works by Clarence and Malan (1957) already suggested that lower positive charge centre (LPCC) is essential for the initiation of CG lightning. On the other hand, an excessive LPCC may prevent the occurrence of CG flashes by ‘‘blocking’’ the progression of descending negative leaders from reaching ground (Qie et al 2005, Nag and Rakov, 2009). In this regard, it is worth noting certain differences between the analysed episodes. Lighting to WT on the 20th November, 18th January and 3rd April episodes correspond mainly to CG flashes starting with negative leaders vertically descending to ground. According to the CG classification based on the magnitude of the LPCC by Nag and Rakov (2009), this behaviour suggests a relatively thin LPCC, where the descending negative leader would traverse the positive charge region keeping a predominantly vertical propagation direction towards the ground. Regarding precipitation structure, this “vertical” negative CG flashes tended to have their origin on

the periphery of convective cores. Studies like Carey et al. (2003), Lund et al. (2007) and Akita et al. (2011) pointed out these areas along the perimeter of updrafts as prone to originate CG lightning. Contrarily, lightning strokes to WT on the 17th November show significant horizontal propagation before reaching ground, suggesting a larger LPCC compared to the precedent cases. According to the Nag and Rakov (2009) classification, in this scenario, a negatively-charged leader channel originated in the base of the main negative charge region would travel predominantly horizontally because of the blocking LPCC effect, eventually making a termination to ground.

Thirdly, the 16th November 2013 episode presented a particular structure, with two layers of opposite polarity and no apparent lower positive layer. The structure on that day had common features with what has been observed, also with an LMA, by Wang et al. (2017) in winter thunderstorms in Japan: (i) an horizontal extension much larger than the vertical extension (a large-scale stratiform cloud with relatively weak echo intensity and low cloud top height (ii) the charge regions enclosed between the –10ºC and –20ºC isotherms, in agreement with the NIC, and (iii) a low altitude of the whole cloud, with positive charge over negative charge. This particular charge distribution has also been reported by Schultz et al. (2011) for upwards from high towers during electrified snowfall events. All in all, this particular scenario featured favourable conditions for the self-initiation of UL. Finally, it is worth mentioning that the LMA system can infer the charge structure only when lightning occurs. In this particular case, the lightning rate was very small, so the charge structure inferred from LMA sources cannot be seen as the complete picture of the thunderstorm charge structure.

4.2. Transition season thunderstorms

Results presented bring new evidence on the low correlation existing between lightning incidence on WT and the month average lightning density for the region surrounding the wind farm. Results point out that lightning activity in the AoS concentrates between June and October (85% of the year-round CGs) and especially during August and September (57% of CGs). However, all the analysed episodes with lightning from/to WT occurred between November and April, months that account only for nine percent of the year-round lightning activity.

Other studies on lightning incidence to tall structures have shown a similar pattern. For instance, studies at the Gaisberg Tower (Montanyà et al., 2007; Diendorfer, 2009) have shown that although the thunderstorm season in Austria is between April and August, actually the months with the highest numbers of recorded flashes at the Gaisberg tower are March and November, respectively, which are definitely months outside the convective season and generally with very little thunderstorm activity in Austria (Diendorfer, 2017). Other studies in towers around Europe also registered a majority of self-initiated flashes during the winter period, such as the Peissenberg Tower (Manhardt et al., 2012). On the contrary, the majority of upward flashes at the Säntis Tower occur during summer (Romero et al., 2013; Smorgonskiy et al., 2015) like in Rapid City (Warner et al., 2012a, b). According to Smorgonskiy et al. (2015) seasonal variations could be attributed to the differences in the tower effective height, although they pointed out that further research is needed to validate this hypothesis.

Going back to the present results, with the exception of the January case, the rest occurred during the transition from summer to winter and vice versa. During these transition periods, at most mid-latitude locations, like the AoS, the lower boundary of the mixed phase region (i.e., the –10 °C isotherm) suffers a sudden change of height. Fig.14 shows the average evolution of the height of the –10 °C isotherm throughout the year near the AoS (calculated from the Barcelona radiosounding database). The average over a 10–year period (2006–2015) indicates that the –10°C isotherm is between 5.5 and 6 km height during the

thunderstorm season (June-September) and around 4 km height in winter (December to March). Interestingly, most of the episodes with lightning to WT have been observed during the transitional season, when the isotherm –10°C is approximately 1.5 km below the typical thunderstorm season and therefore closer to ground.

4.3. Morphology and Size of the storm

Results showed that the storms involved in lightning strokes to WT had no particular precipitation structure, developed in a weak convective environment and had modest amounts of lightning. Recently, Wang et al. (2017) pointed out the preference of CG lightning for regions with weak updraft and downdraft. In the present case study, the majority of downward lightning striking WTs are linked to weak convective cores embedded into stratiform dominant systems.

Interestingly, some of the analysed case studies also produced sprites, episodes which are analysed in detail in Van de Velde et al. (2014). There are other studies that reported sprite-parent +CGs involved also in UL (Warner et al., 2011; Lyons et al., 2011 and 2014). High peak current +CGs are followed by long continuing currents, thus resulting in large charge moment changes (CMC) capable of producing transient luminous events (TLE) (e.g. sprites, elves, halos) as documented in different studies (Takahashi et al., 2003; Suzuki et al., 2006; Matsudo et al., 2007; Van de Velde et al., 2014). It is worth stressing out that in our cases most storm systems were relatively small (see dimensions in Table 1) compared to other TLE-related systems like those documented in the central United States (e.g., Lyons, 1996; Lyons et al., 2003; Lang et al., 2010, 2011; Lu et al., 2013). Thunderstorms like 20th November, 3rd April and 17th November exhibited slow storm motion and weak organization in the absence of a strong cold pool, having only weak updrafts in the humid, low energy environment (van der Velde et al 2014). In any case, the stratiform region of these thunderstorms may grow large enough to allow the necessary charge moment change to trigger a sprite. Regarding the SIUL episode, the 16th November 2013, the storm system area is significantly larger than the rest of episodes.

4.4. Peak current and polarity

CG peak current and polarity reported on Table 1 corresponding to the CGs to WT show that almost all downward strokes had negative polarity (only one positive case), with rather high peak currents. According to the SMC-LLS records, the average (and median) for Catalonia over the last 7 years (2010–2016) for negative CG strokes is of –18.2 kA (–12.9 kA). In the present study, fifteen of the twenty-two negative downwards to WT had peak currents above the average, and furthermore, in 8 cases the peak current is extremely high (above the 95 percentile, –48 kA). These figures suggest that the peak current plays a role on the attachment process to WT. The distance between the tips of the negative downward leaders and the grounded structure (striking distance, Golde 1945), can be estimated using expressions that relate this distance and the peak current (Love 1973, Cooray et al. 2007) The striking distance increases with increasing peak current (Love 1973, Wang et al. 2013, Tran and Rakov 2015, Visacro et al. 2016), thus favouring the attachment to salient objects like WT.

4.5. Self-initiated and Lightning-triggered upwards

As stated in the introduction, upward lightning (UL) may originate from WT due to locally strong electric fields (self-initiated upward lightning, SIUL) or may be triggered by prior lightning discharges (lightning-triggered upward lightning, LTUL). In our case study, all SIUL cases were reported during a single episode,

the 16th November 2013. Complementary data from LMA and LINET allows to confirm the absence of a pre-existing lightning (IC or CG) in the vicinity that may have triggered those upwards. Vertical trails of the SIUL flashes detected on that day (Fig. 10) are similar to LMA observations reported by Schultz et al (2011) during a thundersnow. In both cases, upward flashes start with a series of very low altitude pulses, followed by a upward negative leader that reaches the upper positive layer. This sequence may be repeated in time, starting from other turbines of the wind farm. The 16th November 2013 episode has very low cloud bases, low freezing levels and a considerable stratiform region (more than 30,000 km^2, 2 to 7 times more than the "downward" cases). Under these conditions, the electric field above the WT may become large enough to initiate breakdown, and an upward leader may initiate even without additional transient enhancement from a nearby CG or IC lightning discharge. According to Yuan et al. (2017), the relatively low lightning frequency may have facilitated the efficient charge accumulation in the stratiform cloud, favouring the upward leader inception.

On the other hand, Warner et al. 2014 pointed out that strong ambient winds may not be essential for the triggering as SIULs could originate from rotating turbine blade tips at almost any ambient wind velocity. Wang and Takagi (2012) also noted that self-initiation occurred with higher observed wind speeds (or a rotating windmill) compared with other-triggered upward flashes. The underlying reason would be the wind removal of the screening layer present near the tip of the tower that acts as an inhibitor of the upward leader initiation. Unfortunately, for our case studies we do not have wind records from the windfarms to analyse the possible influence of the wind speed.

In Wang and Takagi (2012), LTUL flashes occurred during taller and more active storms, whereas the majority of SIUL took place when there was not significant lightning activity. In our cases studies, Fig.13 shows a thinner and lower charge structure for the SIUL triggering episode, as well as intermediate conditions for the downward/LTUL episodes, compared to the higher typical summer charge structure. On the other hand, LFR in the AoS were similar in both SIUL and LTUL episodes, the difference being the distance between the embedded convective cores and the wind farms. Downward strokes and LTUL from WT emanate from the vicinity of convective cores, whereas on the 16 November SIUL occurred far from the embedded cores of the precipitation system (50 km approx.).

4.6. Risk assessment

Since the availability of simultaneous observations of weather radar and LLS became available for the analysis of life-cycle of the thunderstorms, different studies have attempted to establish links between radar reflectivity, environmental temperature profiles and lightning. Lang and Rutledge (2011), summarizing on earlier studies, state that the general scope is that the existence of a 40 dBZ echo at or above the altitude of –10°C corresponds to a very high probability of lightning. The present analysis has shown that, as a general rule, LMA detections are limited to periods when the TOP–12 lies above the –10°C height. Moreover, VHF source's density showed a close relation with the height of the TOP–35. Surges in the number of sources detected by the LMA are usually observed shortly after the TOP–35 overtakes the –10°C height, and larger densities are collocated in time with greater heights of the TOP–35, which can reach the –40°C in the summer cases. In a similar way, lightning activity decreases as the TOP–35 losses height and ceases as the TOP–12 decays below the –10°C height. These conditions have been observed in all case studies, and therefore results suggest that they apply throughout the year. This pattern can be of utility in lightning hazard warning systems devoted to wind farms, considering that damage to WT is not solely linked to deep convection or severe weather conditions but also to low-intensity thunderstorms outside the main thunderstorm season.

On the other hand, whereas empirical formulas have been developed to estimate the number of downward flashes to a tall object, the majority of the strokes to modern turbines are expected to be UL. In this regard, it is worth recalling that upward leaders not followed by return strokes can go unnoticed by conventional LLS, and therefore the number of UL is being underestimated (e.g. March 2017). As Rachidi et al. (2008) pointed out, neglecting upward flashes, as done in practice nowadays, might result in an important underestimation of the actual number of strokes to WT. The present results provide evidence supporting this statement, as lightning that may pose a threat to wind turbines is linked to "out of season" low-intensity thunderstorms, which are not a significant contribution to the lightning climatology of the region, in terms of the amount of lightning and therefore the region's average flash density, which is the main lightning parameter used in risk assessment.

5. CONCLUDING REMARKS

The meteorological conditions and thunderstorm characteristics favouring lightning to wind turbines have been analysed in a series of episodes, by means of Lightning Mapping Array and weather radar data. The main takeaways of this study are summarized hereunder.

- As a general rule, lightning activity can be expected in cells where the radar TOP–12 product (height of the echo-tops >12 dBZ) is above the –10°C height. Besides, the TOP–35 reaching the –40°C is indicative of deep convection and large lightning intensities will follow. This rule of thumb applies throughout the year and may be useful to identify thundery conditions that can pose a threat to wind turbines outside the main thunderstorm season

- Lightning threats to wind turbines in the area of study do not occur during the main thunderstorm season, but during transitional periods (spring and autumn). Lightning activity in the area of study concentrates between June and October (85% of the year-round CGs) and especially during August and September (57% of CGs). However, all the analysed episodes with lightning from/to wind turbines occurred between November and April, months that account only for nine percent of the year-round lightning activity.

- Thunderstorms with downward lightning to wind turbines present a regular charge layer structure (tripole), but with particular features. The dominant charge layer is the lower positive one, which is, in turn, closer to the ground due to the environmental temperature. Besides, the reported downward CGs striking WT were mainly of negative polarity and with peak currents above the average.

- Conditions for self-initiated upward lightning from wind turbines were different, with a considerable stratiform region with a low cloud base, bearing a two layer charge structure with positive over negative charge. Such characteristics are similar to those reported for upward lightning in winter thunderstorms in Japan and the US

- Although the thunderstorms involved in lightning incidence on wind turbines had no particular precipitation structure, downwards to wind turbines are related to convective cores embedded in a dominant stratiform region. This stratiform field may grow large enough to allow the necessary charge moment change to trigger upwards from the wind turbines.

- The particular conditions that lead to lightning strokes to wind turbines shall be taken into account in the lightning protection standards, which currently seem to be underestimating the actual number of strokes to wind turbines.

6. ACKNOWLEDGEMENTS

The authors are grateful to the Meteorological Service of Catalonia for providing radar, lightning and radiosonde data. We thank Patricia Altube and the two anonymous reviewers for their comments, that led to further refinement of this study. This work was supported by research grants from the Spanish Ministry of Economy and Competitiveness (MINECO) and the European Regional Development Fund (FEDER): (MINECO) AYA2011-29936-C05-04; (MINECO/FEDER) ESP2013- 48032-C5-3-R and (MINECO/FEDER) ESP2015-69909-C5-5-R; as well as by Fulgura S.L., the Meteorological Service of Catalonia and the Autonomous Government of Catalonia, under the framework of the Industrial Doctorate Programme.

7. REFERENCES

Abellán, E., Aran, M., Codina, B., Cunillera, J., 2011. Complex quality control of Barcelona radiosounding database. 6th European Conference on Severe Storms (ECSS) 2011, Palma de Mallorca, Spain.

Akita, M., Yoshida, S., Nakamura, Y., Morimoto, T., Ushio, T., Kawasaki, Z., Wang, D., 2011. Effects of charge distribution in thunderstorms on lightning propagation paths in Darwin, Australia. J. Atmos. Sci., 68, 719–726, doi.org/10.1175/2010JAS3597.1

Altaratz, O., Levin, Z., Yair, Y., 1999. Electrical and radar observation of thunderstorms in the eastern Mediterranean. Preprints, 11th Int. Conf. on Atmospheric Electricity, Guntersville, AL, ICAE, 468–471.

Altaratz, O., Levin, Z., Yair, Y., 2001. Winter Thunderstorms in Israel: A Study with Lightning Location Systems and Weather Radar. Mon. Weather Rev., 129, 1259–1266.

Argemí, O., Altube, P., Rigo, T., Ortiga, X., Pineda, N., Bech, J., 2014. Towards the improvement of monitoring and data quality assessment in the weather radar network of the Meteorological Service of Catalonia, 8th European Conference on Radar in Meteorology and Hydrology (ERAD), Garmisch-Partenkirchen, Germany, Sept. 2014

Bech, J., Vilaclara, E., Pineda, N., Rigo, T., López, J., O'Hora, F., Lorente, J., Sempere, D., Fàbregas, F.X., 2004. The weather radar network of the Catalan Meteorological Service: description and applications. Proceedings of the 3rd European Conference on Radar (ERAD 2004), Copernicus GmbH.

Berger, K., 1967. Novel observations on lightning discharges: Results of research on Mount San Salvatore, J. Franklin Inst., 283, 478–525, doi:10.1016/0016-0032(67)90598-4.

Betz, H.D., Schmidt, K., Oettinger, P., Wirz, M., 2004. Lightning detection with 3-D discrimination of intracloud and cloud-to-ground discharges. Geophys. Res. Lett., 31, L11108, doi:10.1029/2004GL019821.

Betz, H.D., Schmidt, K., Laroche, P., Blanchet, P., Oettinger, W.P., Defer, E., Dziewit, Z, Konarski, J., 2009a. Linet—An international lightning detection network in Europe. Atmos. Res., 91: 564 –573. doi:https://doi.org/10.1016/j.atmosres.2008.06.012

Betz, H.D., Schmidt, K, Oettinger, W.P. 2009b. LINET: An international VLF/LF lightning detection network in Europe. Springer, 2009b. In: Betz, H.-D., Schumann, U., Laroche, P. (Eds.), Lightning: Principles, Instruments and Applications. Springer, Netherlands, pp. 115–140.

Braam, H., Rademakers, L.W.M.M., Wessels, H.R.A., Prins, R.K.N.J., Lok., R., Leunis, L., Ramakers, S.G.M., 2002. Lightning damage of OWECS Part 3: Case studies, published by ECN (www.ecn.nl), Netherlands

Buechler, D.E., Goodman, S.J., 1990. Echo Size and Asymmetry: Impact on NEXRAD Storm Identification. J. Appl. Meteor., 29, 962–969

Candela, A., Madsen, S.F., Nissim, M., Myers, J.D., Holboell, J., 2016. Lightning Damage to Wind Turbine Blades From Wind Farms in the U.S. IEEE Trans. Power Del., 31(3): 1043

Carey, L.D., Petersen, W.A.; Rutledge, S.A., 2003. Evolution of cloud-to-ground lightning and storm structure in the Spencer, South Dakota, Tornadic Supercell of 30 May 1998. Mon. Weather Rev. 131, 1811–1831.

Chan, M.-K., Chen, M., Du, Y-P., 2018. A macroscopic physical model for self-initiated upward leaders from tall grounded objects and its application. Atmos. Res., 200, 13–24.

Cummins, K.L., Murphy, M.J., 2009. An overview of lightning locating systems: history, techniques, and data uses, with an in-depth look at the U.S. NLDN. IEEE Trans. Electromagn. Compat. 51 (3), 499–518.

Clarence, N.D., Malan, D.J., 1957. Preliminary discharge processes in lightning flashes to ground, Q. J. R. Meteorol. Soc., 83, 161–172.

Cooray, V., Rakov, V., Theethayi, N., 2007. The lightning striking distance—Revisited. J. Electrostat. 65(5–6), 296–306. doi.org/10.1016/j.elstat.2006.09.008

Diendorfer, G., Pichler, H., Mair, M., 2009. Some parameters of negative upward-initiated lightning to the Gaisberg Tower (2000–2007). IEEE Trans. Electromagn. Compat. 51, 443–452.

Diendorfer, G., Pichler, H., Schulz, W., 2014. EUCLID Located Strokes to the Gaisberg Tower – Accuracy of Location and its assigned Confidence Ellipse. In: Int. Lightning Detection Conf. and Int. Lightning Meteorology Conf. (ILDC/ILMC), Tucson, 2014.

Diendorfer, G. 2017. Review of seasonal variations in occurrence and some current parameters of lightning measured at the Gaisberg Tower. 4th Int. Symposium on Winter Lightning (ISWL 2017), Joetsu, Japan.

Duda, J.D., Gallus, W.A., 2010. Spring and Summer Midwestern Severe Weather Reports in Supercells Compared to Other Morphologies. Wea. Forecasting, 25, 190–206.

Dye, J.E., Jones, J.J., Winn, W.P., Cerni, T.A., Gardiner, B., Lamb, D., Pitter, R.L., Hallett, J.,Saunders, C.P.R., 1986. Early electrification and precipitation development in a small, isolated Montana cumulonimbus. J. Geophys. Res. 91, 1231–1247.

Eriksson, A. J., 1978. Lightning and tall structures, Trans. S. Afr. Inst. Electr. Eng., vol. 69, pp. 238–252.

Foley, A.M., Leahy, P.G., Marvuglia, A., McKeogh, E.J., 2012. Current Methods and Advances in Forecasting of Wind Power Generation. Renewable Energy, 37, 1-8.

Galanaki, E., Lagouvardos, K., Kotroni, V., Flaounas, E., Argiriou, A., 2018. Thunderstorm climatology in the Mediterranean using cloud-to-ground lightning observations, Atmos. Res., 207: 136-144

Golde, R. H., 1945. The frequency of occurrence and the distribution of lightning flashes to transmission lines. Electrical Engineering, 64(12): 902–910. doi.org/10.1109/EE.1945.6441405

Gremillion, M, Orville, R, 1999. Thunderstorm Characteristics of Cloud-to-Ground Lightning at the Kennedy Space Center, Florida: A Study of Lightning Initiation Signatures as Indicated by the WSR-88D. Amer. Meteor. Soc., 14, 640-649.

Hondl, K., Eilts, M., 1994. Doppler radar signatures of developing thunderstorms and their potential to indicate the onset of cloud-to-ground lightning. Mon. Weather Rev., 122, 1818-1836.

Honjo, N., 2015. Risk and its reduction measure for wind turbine against the winter lightning, in Proc. Asia-Pacific Intl. Conf. on Lightning, 2015, pp. 665-670.

IEC 61400-24, Wind Turbines – Part 24: Lightning Protection, 2010.

Jacobson, E.A., Krider, E.P., 1976. Electrostatic field Changes produced by Florida lightning, J. Atmos. Sci., 33, 103-117

Kotroni, V., Lagouvardos, K., 2016. Lightning in the Mediterranean and its relation with sea-surface temperature. Environ. Res. Lett. 11, 034006. http://dx.doi.org/10.1002/asl.685.

Krehbiel, P. R., 1986: The electrical structure of thunderstorms. In: The Earth's Electrical Environment, National Academies Press, 90–113.

Krehbiel, P.R., Brook, M., Khanna-Gupta, S., Lennon, C. L., Lhermitte, R., 1984. Some results concerning VHF lightning radiation from the real-time LDAR system at KSC, Florida. Proc. 7th Int. Conf. on Atmospheric Electricity, Boston, MA, Amer. Meteor. Soc., 388–393

Lang, T.J. Rutledge, S.A., 2011. A Framework for the Statistical Analysis of Large Radar and Lightning Datasets: Results from STEPS 2000. Mon. Weather. Rev., 139, 2536–2551

Lang, T.J., Lyons, W.A., Rutledge, S.A., Meyer, J.D., MacGorman, D.R., Cummer, S.A., 2010. Transient luminous events above two mesoscale convective systems: Storm structure and evolution, J. Geophys. Res., 115, A00E22, doi:10.1029/2009JA014500.

Lang, T.J., Li, J., Lyons, W.A., Cummer, S.A., Rutledge, S.A., MacGorman, D. R., 2011. Transient luminous events above two mesoscale convective systems: Charge moment change analysis, J. Geophys. Res., 116, A10306, doi:10.1029/2011JA016758.

Larsen, H.R., Stansbury, E.J., 1974. Association of lightning flashes with precipitation cores extending to height 7 km. J. Atmos. Terr. Phys. 36, 1547–1553.

Levin, Z., Yair, Y., Ziv, B., 1996: Positive cloud-to-ground flashes and wind shear in Tel-Aviv thunderstorms. Geophys. Res. Lett., 23, 2231–2234.

Love, E.R., 1973. Improvements on lightning stroke modeling and applications to the design of EHV and UHV transmission lines, University of Colorado.

Lund, N., and Coauthors, 2007. Relationship between lightning location and polarimetric radar signatures in an MCS. Proc. 13th Int. Conf. on Atmospheric Electricity, Beijing, China, ICAE, 557–560.

Lu, G., et al., 2013. Coordinated observations of sprites and in-cloud lightning flash structure, J. Geophys. Res. Atmos., 118, 6607–6632, doi:10.1002/jgrd.50459

Lyons, W.A., 1996. Sprite observations above the U.S. High Plains in relation to their parent thunderstorm systems, J. Geophys. Res., 101, 29,641–29,652, doi:10.1029/96JD01866.

Lyons, W.A., Williams, E. R., Cummer, S. A., Stanley, M. A., 2003. Characteristics of sprite-producing positive cloud-to-ground lightning during the 19 July 2000 STEPS mesoscale convective systems, Mon. Weather Rev., 131, 2417–2427.

Lyons, W.A., Cummer, S.A., Rutledge, S.A., Lang, T.J., Meyer, T., Warner, T.A., Samaras, T.A., 2011. TLEs and their parent lightning discharges, paper presented at 14th International Conference on Atmospheric Electricity (ICAE), Rio De Janeiro, Brazil, 7–12 Aug.

Lyons, W.A., et al., 2014. Meteorological Aspects of Two Modes of Lightning-Triggered Upward Lightning (LTUL) Events in Sprite-Producing MCS, 23rd Int. Lightning Detection Conf., 18-19 March 2014, Tucson, Arizona.

MacGorman, D.R., Rust, W.D.,1998. The Electrical Nature of Storms, 422 pp., Oxford Univ. Press, Oxford.

Manhardt, M., Heidler, F., Stimper, K., 2012. The electric field of negative upward lightning strikes at the Peissenberg tower, Germany. Int. Conf. on Lightning Protection (ICLP), 2012, IEEE,pp.1–9. 10.1109/ICLP.2012.6344205.

March, V., 2017. Key issues to define a method of lightning risk assessment for wind farms, Electr. Power Syst. Res., doi:10.1016/j.epsr.2017.08.020

Marshall, T.C., Stolzenburg, M., 2002. Electrical energy constraints on lightning. J. Geophys. Res. 107 (D7). doi:10.1029/2000JD000024.

Matsudo, Y., Suzuki, T., Hayakawa, M., Yamashita, K., Ando, Y., Michimoto, K., Korepanov, V., 2007. Characteristics of Japanese winter sprites and their parents' lightning as estimated by VHF lightning and ELF transients, J. Atmos. Sol. Terr. Phys., 59, 1431–1446

Mazur, V., 2002. Physical processes during development of lightning flashes, C. R. Phys., 3, 1393–1409.

Mazur, V., Shao, X., Krehbiel, P.R., 1998. "Spider" lightning in intra-cloud and positive cloud-to-ground flashes, J. Geophys. Res., 103, 19,811–19,822, doi: 10.1029/98JD02003.

McEachron, K. B., 1939. Lightning to the Empire State Building, J. Franklin Inst., 227, 149–217, doi:10.1016/S0016-0032(39)90397-2.

Michimoto, K., 1991: A study of radar echoes and their relation to lightning discharge of thunderclouds in the Hokuriku district, Part 1: Observation and analysis of thunderclouds in summer and winter. J. Meteor. Soc. Japan, 69, 327–335.

Michimoto, K., 1993. A study of radar echoes and their relation to lightning discharge of thunderclouds in the Hokuriku district, Part 2: Observation and analysis of ''single flash'' thunderclouds in midwinter. J. Meteor. Soc. Japan, 71, 195–203.

Minowa, M, Minami, M, Yoda, M., 2006. Research into Lightning Damages and Protection Systems for Wind Power Plants in Japan. Proceedings of the 28th International Conference on Lightning Protection, Kanazawa, 2006; 1539–1544.

Montanyà, J., Pineda, N., March, V., Illa, A., Romero, D., Solà, G., 2006. Experimental evaluation of the Catalan Lightning Detection Network. 19th Int. Lightning Detection Conf., Tucson, Arizona.

Montanyà, J., Soula, S., Diendorfer, G., Solà, G., Romero, D., 2007. Analysis of altitude of isotherms and the electrical charge for flashes that struck the Gaisberg Tower. 13th International Conference on Atmospheric Electricity (ICAE), August 13-17 2007, Beijing, China.

Montanyà, J., van der Velde, O.A., March, V., Romero, D., Solà, G., Pineda, N., 2012. High-speed video of lightning and x-ray pulses during the 2009–2010 observation campaigns in north-eastern Spain. Atmos. Res. 117, 91–98.

Montanyà, J., 2014. Annual Report on the Performance of the Lightning Location System Operated by the Meteorological Service of Catalonia, Internal Technical Report, not Published.

Montanyà, J., van der Velde, O., Williams, E. R., 2014. Lightning discharges produced by wind turbines. J. Geophys. Res. Atmos., 119, 1455–1462, doi:10.1002/ 2013JD020225.

Montanyà, J., Fabró, F., van der Velde, O., March, V., Williams, E.R., Pineda, N., Romero, D., Solà, G., Freijo, M., 2016a. Global distribution of winter lightning: a threat to wind turbines and aircraft. Nat. Hazards Earth Syst. Sci., 16, 1465-1472

Montanyà, J., van der Velde, O., Domingo-Dalmau, A., Pineda, N., Argemí, O., Salvador, A., 2016b. Lightning mapping observations of downward lightning flashes to wind turbines. 33rd Int. Conf. Lightning Protection, Estoril, Portugal, 25-30 September 2016.

Murphy, M.J., Krider, E.P., Maier, M.W., 1996. Lightning charge analyses in small Convection and Precipitation Electrification (CaPE) experiment storms, J. Geophys. Res., 101(D23), 29615–29626, doi:10.1029/96JD01538.

Nag, A., Rakov V.A, 2009. Some inferences on the role of lower positive charge region in facilitating different types of lightning, Geophys. Res. Lett., 36, L05815, doi:10.1029/2008GL036783.

Nag, A., Murphy, M. J., Schulz, W., Cummins, K.L., 2015. Lightning locating systems: Insights on characteristics and validation techniques, Earth and Space Science, 2, 65–93, doi:10.1002/ 2014EA000051.

Neubert, T., Kuvvetli, I., Budtz-Jørgensen, C., Østgaard, N., Reglero, V. Arnold, N., 2006. The atmosphere-space interactions monitor (ASIM) for the international space station. ILWS Workshop 2006, GOA, February 19-24, 2006

Parker, M.D., Johnson, R.H., 2000. Organizational modes of mid-latitude mesoscale convective systems. Mon. Weather Rev.,128, 3413–3436

Pawar, S.D., Kamra, A.K., 2004. Evolution of lightning and the possible initiation/triggering of lightning discharges by the lower positive charge center in an isolated thundercloud in the tropics, J. Geophys. Res., 109, D02205, doi:10.1029/2003JD003735.

Pierce, E.T., 1971. Triggered Lightning and Some Unsuspected Lightning Hazards. Stanford Research Institute, Menlo Park, CA, 1971, pp. 20.

Pineda, N., Montanyà, J., 2009. Lightning detection in Spain: the particular case of Catalonia. In: Betz, H.-D., Schumann, U., Laroche, P. (Eds.), Lightning: Principles, Instruments and Applications. Springer, Netherlands, pp. 161–185.

Pineda, N., Soler, X., Vilaclara, E., 2011. Approximation to the Lightning Climatology in Catalonia. Technical Note nº 73. Meteorological Service of Catalonia: 71 p. Generalitat de Catalunya B-7024-2011 (in Catalan)

Poelman, D.R., Schulz, W., Diendorfer, G., Bernardi, M., 2016. The European lightning location system EUCLID – Part 2: Observations. Nat. Hazards Earth Syst. Sci., 16, 607–616, 2016. doi:10.5194/nhess-16-607-2016

Qie, X., Zhang, T., Chen, C., Zhang, G., Zhang, T., Wei, W., 2005. The lower positive charge center and its effect on lightning discharges on the Tibetan Plateau, Geophys. Res. Lett., 32, L05814, doi:10.1029/2004GL022162

Rachidi, F., Rubinstein, M., Montanyà, J., Bermudez, J.L., Rodriguez, R., Solà, G., Korovkin, N., 2008. A review of current issues in lightning protection of new generation wind turbine blades, IEEE Trans. Ind. Electron., vol. 55, no. 6, pp. 2489–2496, doi:10.1109/TIE.2007.896443.

Radicevic, R.M., Savic, M.S., Madsen S.F., Badea I., 2012. Impact of wind turbine blade rotation on the lightning strike incidence—A theoretical and experimental study using a reduced-size model, Energy, 45, 644–654.

Reynolds, S.E., Brook, M., 1956. Correlation of the initial electric field and the radar echo in thunderstorms. J. Meteor. , 13, 376-380.

Rizk, F.A.M. 1990. Modeling of transmission line exposure to direct lightning strokes, IEEE Trans. Power Del. 5 (4): 1983-1997

Rizk, F.A.M., 1994. Modelling of lightning incidence to tall structures, part I & II. IEEE Trans. Power Del. 9 (1): 162-193

Rison, W., Thomas, R.J., Krehbiel, P.R., Hamlin, T., Harlin J., 1999. A GPS-based three-dimensional lightning mapping system: Initial observations in central New Mexico, J. Geophys. Res., 26, 3573-3576.

Rivas Soriano, L. de Pablo F., Tomas, C., 2005. Ten-year study of cloud-to-ground lightning activity in the Iberian Peninsula. J. Atmos. Terr. Phys. 67: 1632–1639

Rakov, V.A., Uman, M.A., 2003. Lightning: Physics and Effects, Cambridge University Press, Cambridge.

Romero, C., Rachidi, F., Paolone, M., Rubinstein. M., 2013. Statistical Distributions of Lightning Currents Associated With Upward Negative Flashes Based on the Data Collected at the Säntis (EMC) Tower in 2010 and 2011. IEEE Trans. Power Del., 28(3)

Saunders, C.P.R., Bax-Norman, H., Emersic, C., Avila, E.E., Castellano, N.E., 2006. Laboratory studies of the effect of cloud conditions on graupel/ crystal charge transfer in thunderstorm electrification. Q. J. Roy. Met. Soc. 132, 2653–2673.

Schultz, C.J., Bruning, E.C., Carey, L.D., Petersen, W.A., Heckman, S., 2011. Total lightning within electrified snowfall using LMA, NLDN, and WTLN measurements. Eos. Trans. AGU, Fall Meet. Suppl.

Shao, X., Krehbiel, P., 1996. The spatial and temporal development of intracloud lightning, J. Geophys. Res., 101, 26,641–26,668, doi:10.1029/ 96JD01803

Shindo, T., Sekioka, S., Ishi, M., Shiraishi, H., Natsuno, D., 2012. Studies of lightning protection design for wind power generation systems in Japan, CIGRE 2012, C4 306.

Smorgonskiy, A., Tajalli, A., Rachidi, F., Rubinstein, M., Diendorfer, G., Pichler, H., 2015. An analysis of the initiation of upward flashes from tall towers with particular reference to Gaisberg and Säntis Towers, J. Atmos. Terr. Phys. 136(A): 46-51

Stackpole, J.D., 1967. Numerical analysis of atmospheric soundings. J. Appl. Meteor., 6, 464–467.

Suzuki, T., Hayakawa, M., Matsudo, Y., Michimoto, K. 2006, How do winter thundercloud systems generate sprite-inducing lightning in the Hokuriku area of Japan?, Geophys. Res. Lett., 33, L10806, doi:10.1029/2005GL025433.

Takahashi, T., 1978: Riming electrification as a charge generation mechanism in thunderstorms. J. Atmos. Sci., 35, 1536-1548.

Takahashi, Y., Miyasato, R., Adachi, T., Adachi, K., Sera, M., Uchida, U., Fukunishi, H., 2003. Activities of sprites and elves in the winter season, Japan, J. Atmos. Sol. Terr. Phys., 65: 551–560.

Thomas, R., Krehbiel, P.R., Rison,W., Hunyady, S.J.,Winn, W.P., Hamlin, T., Harlin, J., 2004. Accuracy of the lightning mapping array. J. Geophys. Res. 109, D14207. doi:10.1029/2004JD004549

Tomine, K., Michimoto, K., Abe, S., 1986. Studies on thunderstorm in winter in the area surrounding Komatsu by radar (in Japanese). Tenki, 33, 445–452.

Tran, M.D., Rakov, V.A., 2015. When does the lightning attachment process actually begin? Journal of Geophysical Research: Atmospheres, 120, 6922–6936. doi.org/10.1002/2015JD023155

van der Velde, O.A., Montanyà, J., Romero, D., Pineda, N., Rico, R., Fabró, F., Solà, G., March, V., Soula, S., 2011. Results of the 2010-2011 lightning measurement campaigns in Spain, 6th European Conf. on Severe Storms, Palma de Mallorca, Spain, 3-7 October 2011

van der Velde, O.A., Montanyà, J., 2013. Asymmetries in bidirectional leader development of lightning flashes, J. Geophys. Res. Atmos., 118, doi:10.1002/2013JD020257.

van der Velde, O.A., J. Montanyà, S. Soula, N. Pineda, and J. Mlynarczyk, 2014. Bidirectional leader development in sprite-producing positive cloud-to-ground flashes: Origins and characteristics of positive and negative leaders, J. Geophys. Res. Atmos., 119, 12,755–12,779, doi:10.1002/ 2013JD021291.

Vincent, B.R, Carey L.D., Schneider, D., Keeter, K., Gonski, R., 2003. Using WSR-88D reflectivity data for the prediction of cloud-to-ground lightning: A North Carolina study. Nat. Wea. Digest, 27, 35-44.

Visacro, S., Guimaraes, M., Murta Vale, M.H., 2017. Striking distance determined from high-speed videos and measured currents in negative cloud-to-ground lightning. J. Geophys. Res. Atmos., 122, 13,356–13,369. doi.org/10.1002/2017JD027354

Wallace, J.M., Hobbs, P.V., 1973. Atmospheric Science, An Introductory Survey, International Geophysics, vol. 92, 2nd ed., 504 pp., Academic Press, New York.

Wang, D., Takagi, N., Watanabe, T., Sakurano, H., Hashimoto M., 2008. Observed characteristics of upward leaders that are initiated from a windmill and its lightning protection tower. Geophys. Res. Lett., 35, L02803, doi:10.1029/2007GL032136

Wang, D., Takagi, N., 2012. Characteristics of winter lightning that occurred on a windmill and its lightning protection tower in Japan, IEEJ Trans. Power Energy, 132(6), 568–572, doi:10.1541/ieejpes.132.568.

Wang, D., Takagi, N., Gamerota, W.R., Uman, M.A., Hill, J.D., Jordan, D.M., 2013. Initiation processes of return strokes in rocket-triggered lightning. Journal of Geophysical Research: Atmospheres, 118, 9880–9888. doi.org/10.1002/jgrd.50766

Wang, D., Wu, T., Takagi, N., 2017. Charge structure of winter thunderstorm in Japan: a review and an update, 4th International Symposium on Winter Lightning, Japan, April 2017.

Wang, C., Zheng, D., Zhang, Y., Liu, L., 2017. Relationship between lightning activity and vertical airflow characteristics in thunderstorms, Atmos. Res., 191, 2017, 12-19

Warner, T.A., Cummer, S.A., Lyons, W.A., Lang, T.J., Orville, R.E., 2011. Coordinated video and RF measurements of positive CGs inducing both sprites and upward tower discharges, paper presented at 5th Conference on Meteorological Applications of Lightning Data, Am. Meteor. Soc., Seattle, Wash.

Warner, T.A., Cummins, K.L., Orville, R.E., 2012a. Upward lightning observations from towers in Rapid City, South Dakota and comparison with National Lightning Detection Network data, 2004–2010, J. Geophys. Res., 117, D19109, doi:10.1029/2012JD018346.

Warner, T.A., Helsdon Jr., J.H. Bunkers, M.J., Saba, M.F., Orville, R.E., 2012b. UPLIGHTS: Upward lightning triggering study. Bull. Am. Meteorol. Soc., 94, 631 –635, doi:10.1175/BAMS-D-11-00252.1.

Williams, E.R., 1989. The tripole structure of thunderstorms. J. Geophys. Res. 94 (D11): 13,151–13,167.

Williams, E.R., 2001. The electrification of severe storms. Severe convective storms, meteor. Monogr., no. 50. Am. Meteorol. Soc. 527–561.

Williams, E.R., Zhang, R., Rydock, J., 1991. Mixed-Phase Microphysics and Cloud Electrification. J. Atmos. Sci., 48, 2195–2203

Williams, E.R., 2018. Lightning Activity in Winter Storms: A Meteorological and Cloud Microphysical Perspective. IEEJ Transactions on Power and Energy 138 (5): 364-373 doi:10.1541/ieejpes.138.364

Workman, E.J., Reynolds, S.E., 1949: Electrical activity as related to thunderstorm cell growth. Bull. Amer.Meteor. Soc., 30,142-149.

Yair, Y., Levin, Z., Altaratz, O., 1998. Lightning phenomenology in the Tel Aviv area from 1989 to 1996. J. Geophys. Res., 103, 9015–9025.

Yasuda, Y., Yokoyama, S., Minowa, M., Satoh, T., 2012. Classification of Lightning Damage to Wind Turbine Blades IEEJ Transactions on Electrical and Electronic Engineering: 559–566, doi:10.1002/tee.21773

Yeung, L.H.Y., Lai, E.S.T., Chiu, S.K.S., 2007. Lightning Initiation and Intensity Nowcasting Based on Isothermal Radar Reflectivity - A Conceptual Model. In: 33rd Int. Conf. on Radar Meteorology, Cairns, Australia, 6-10 August 2007

Yokoyama, S., 2013. Lightning protection of wind turbine blades. Electric Power Systems Research 94 (2013) 3– 9

Yuan, S., Jiang, R., Qie, X., Wang, D., Sun, Z., Liu, M., 2017. Characteristics of upward lightning on the Beijing 325 m meteorology tower and corresponding thunderstorm conditions. Journal of Geophysical Research: Atmospheres, 122. https://doi.org/10.1002/2017JD027198

Zhou, H., Theethayi, N., Diendorfer, G., Thottappillil, R., Rakov, V.A. , 2010. On estimation of the effective height of towers on mountaintops in lightning incidence studies, Journal of Electrostatics 68: 415-418

Zhou, H., Diendorfer, G., Thottappillil, R., Pichler, H., Mair, M., 2012a. Measured current and close electric field changes associated with theinitiation of upward lightning from a tall tower, J. Geophys. Res., 117, D08102, doi:10.1029/2011JD017269.

Zhou, H., Diendorfer, G., Thottappillil, R., Pichler, H., Mair, M., 2012b. Characteristics of upward positive lightning flashes initiated from the Gaisberg Tower, J. Geophys. Res., 117, D06110, doi:10.1029/2011JD016903.

Table 1. Summary of case studies. Information on each episode includes: Instability indices (Convective Available Potential Energy, CAPE; Lifting Condensation Level, LCL) and isotherm heights (−10ºC, −40ºC and tropopause) derived from radio-sounding. Storm system morphology and area (continuous area above 12 dBZ) are derived from radar imagery. Lightning flash rates (CG) are derived from the SMC-LLS. Finally, the time and type of lightning strokes to wind turbines mapped with the LMA are listed (with maximum peak current per CG flash)

	TYPICAL SUMMER CASES		LIGHTNING TO WT				
Episode	02/08/2014	01/07/2014	20/11/2011	03/04/2012	17/11/2012	16/11/2013	18/01/2014
Radiosounding time (UTC)	12:00	12:00	0:00	12:00	0:00	0:00	0:00
Instablity indices CAPE (J kg^{-1})	2,350	1,350	--	390	113	--	--
LCL (m AMSL)	890	890	--	100	340	430	750
Tropopause Height (m AMSL)	11,000	12,000	--	11,000	11,650	8,500	10,250
Isotherm Heights (m AMSL) -10°C	4,550	5,400	3,000	3,900	4,500	3,100	3,800
-40°C	8,700	9,600	7,100	7,900	8,700	7,100	7,600
Radar Morphology	cluster	cluster	parallel	broken line/	parallel	non-linear	leading
	of cells	of cells	stratiform	trailing str.	startiform	conv.syst.	stratiform
Storm system area (km^2) (>12 dBZ)	2,415	1,905	4,450	5,365	11,485	31,050	10,275
Lightning flash rate (LFR) (CG min^{-1})	4-5	2-3	2-3	1-2	1-2	1-2	3-4
Maximum LFR	15	8	8	8	4.5	3	11.5
LFR during strikes to WT	-	-	7	2	3	1.5	4
Lightning to Wind-Turbines	-	-	DW 04:29 (-12)	DW 18:38 (-18)	DW 16:06 (-23)	SIUL 08:13 (-13)	DW 08:40 (-36)
			DW 04:37 (-98)	DW 18:44 (-28)	DW 16:08 (-77)	SIUL 08:37 (+113)	LTUL 09:00 (-24)
time in UTC			DW 04:39 (-135)	DW 19:33 (-103)	DW 16:24 (-35)	SIUL 08:41 (-39)	DW 09:05 (-19)
Downward (DW)			DW 04:45 (-53)	DW 19:40 (-12)	DW 17:10 (-15)		DW 09:37 (-106)
Lightning-triggered upward (LTUL)			DW 06:55 (-31)		DW 17:34 (-138)		DW 09.39 (-127)
Self-initiated upward (SIUL)			DW 06:57 (-14)		DW 17:59 (+12)		
Maximum Peak current (kA) per CG flash			DW 07:11 (-9)				
			DW 07:15 (-24)				

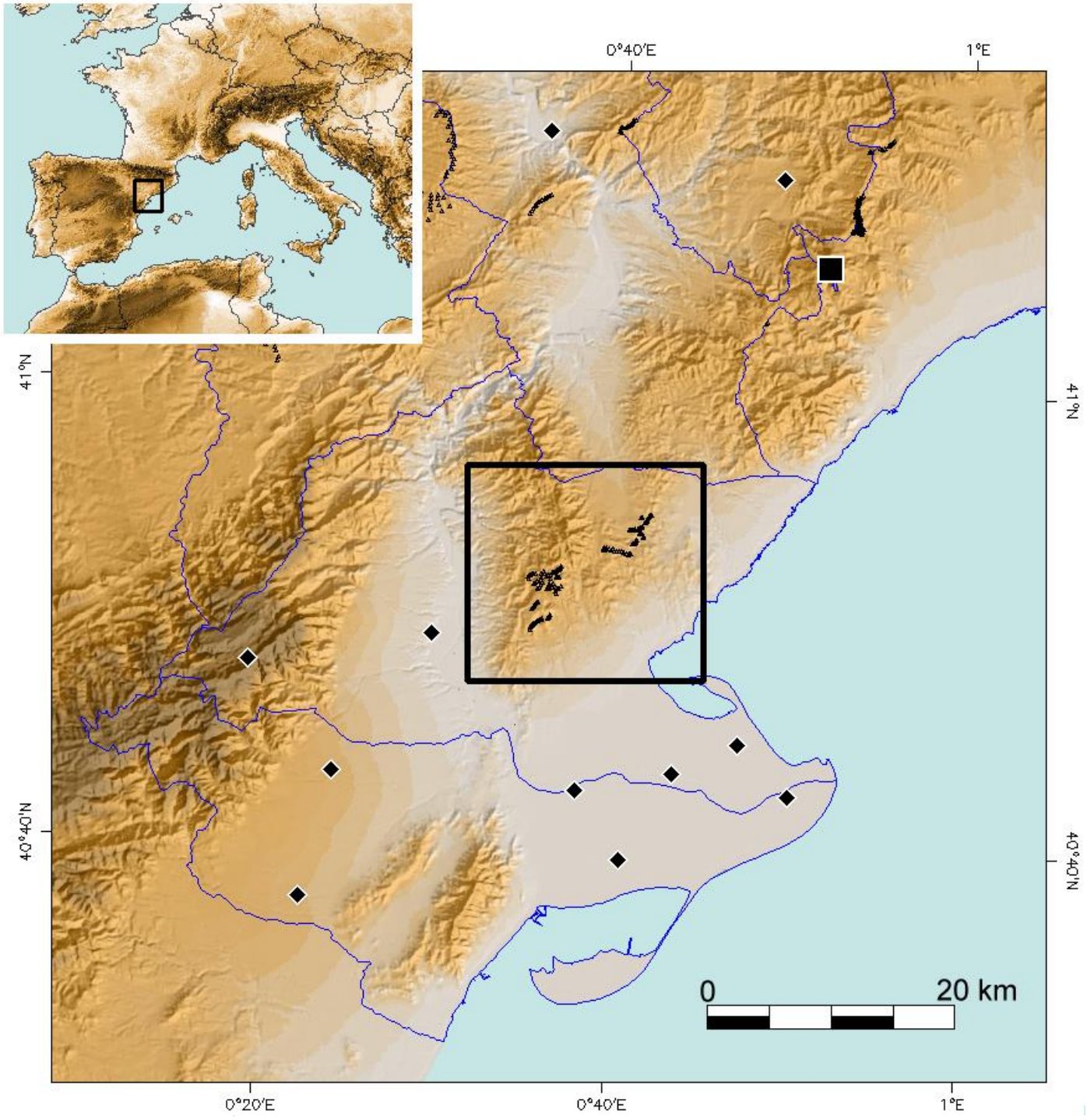

Fig 1. Area of study (AoS), nearby the Ebre's river Delta, south Catalonia, in the Mediterranean coast at the NE of the Iberian Pensinsula . Black diamonds correspond to locations of the *Ebre Lightning Mapping Array* sensors. The black square corresponds to *La Miranda* weather radar site. The highlighted area ecompasses the wind turbines (black triangles) analyzed.

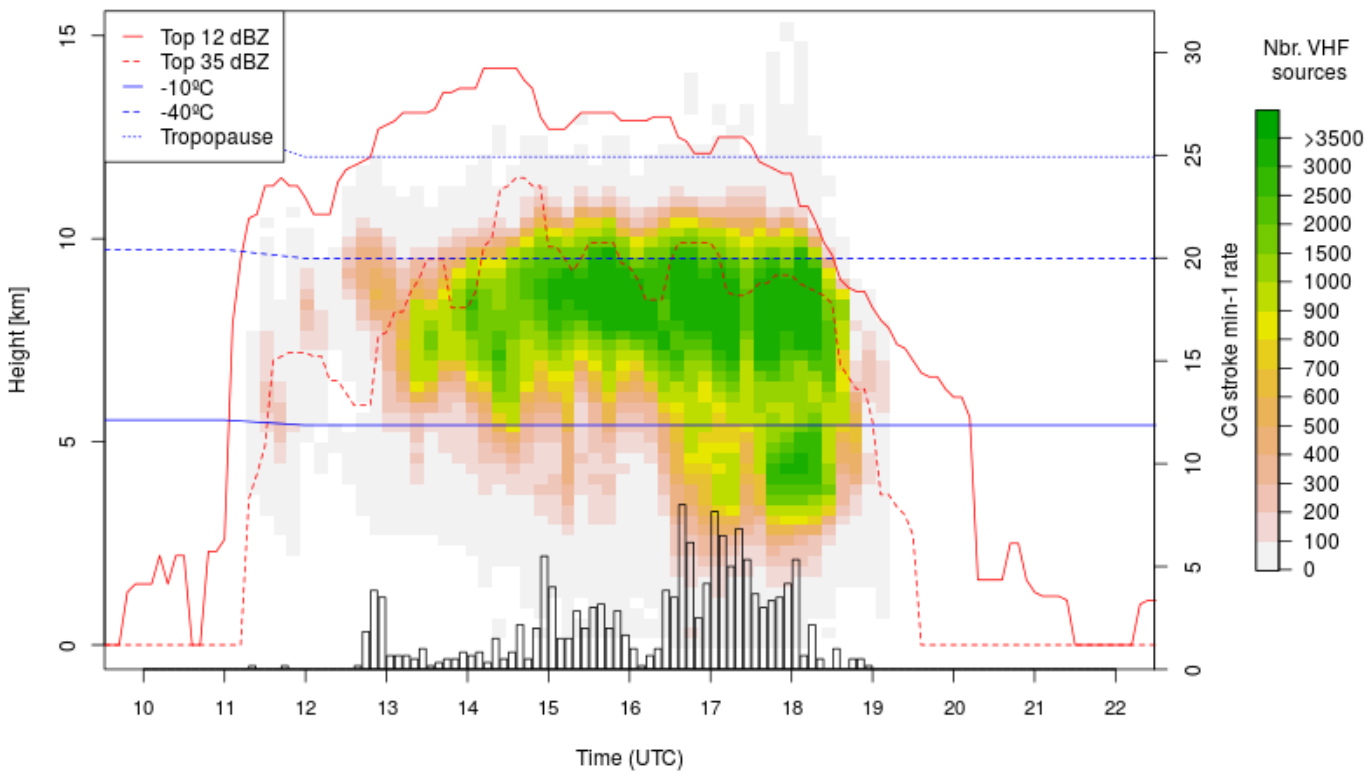

Fig 2. Evolution of the vertical structure of the storms occurring in the area of study on the 1st July 2014. Time–height LMA source density plot. Colour indicates relative density of sources according to a pink-yellow-green colour scheme. The largest source densities are in green. Red lines correspond to the height of the TOP−12 (dashed) and TOP−35 (solid) products. Bar lines indicate the CG flash rate in a 10–min timestamp. Finally, blue lines correspond to the representative environmental temperature values obtained from the vertical sounding profiles (–10°C, –40°C and tropopause heights in km)

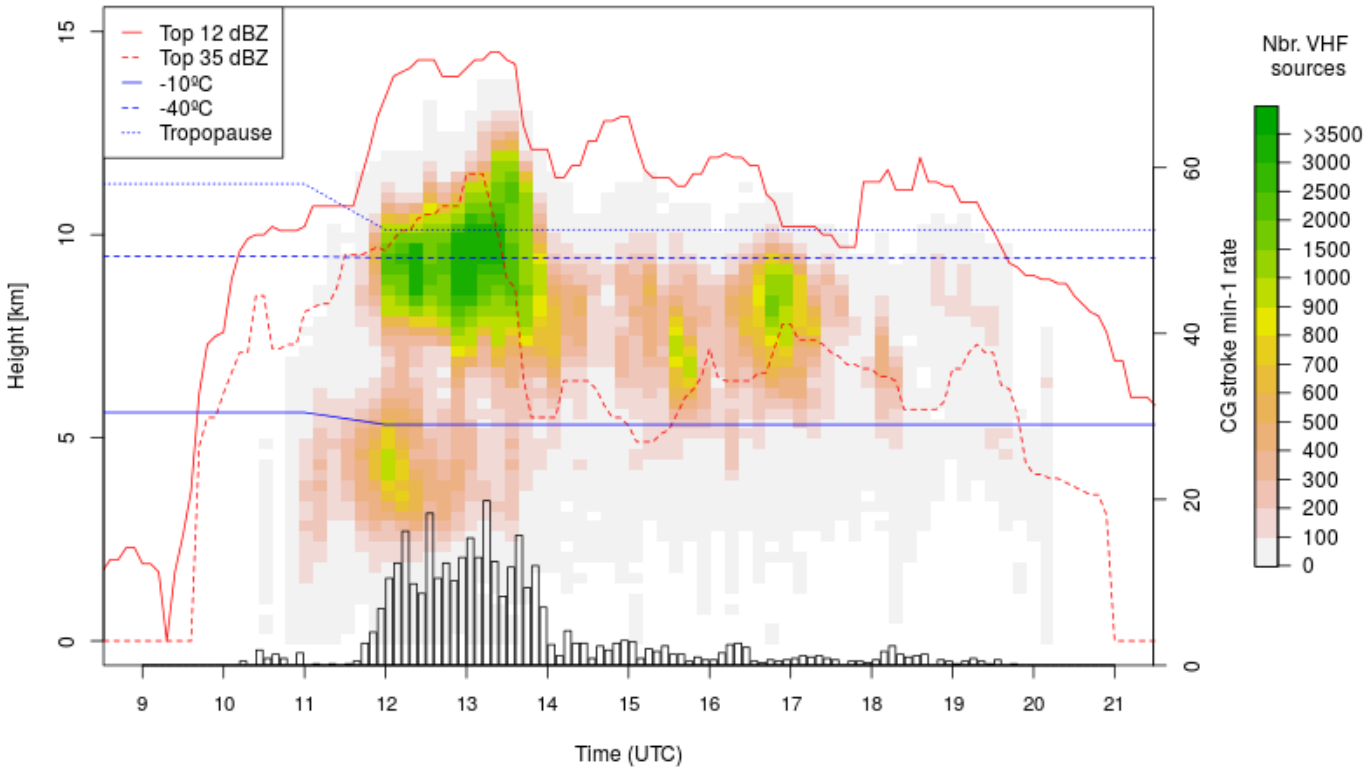

Fig. 3. Analogous to Fig. 2, but showing the evolution of the vertical structure of the storms occurring in the area of study on the 2nd August 2014.

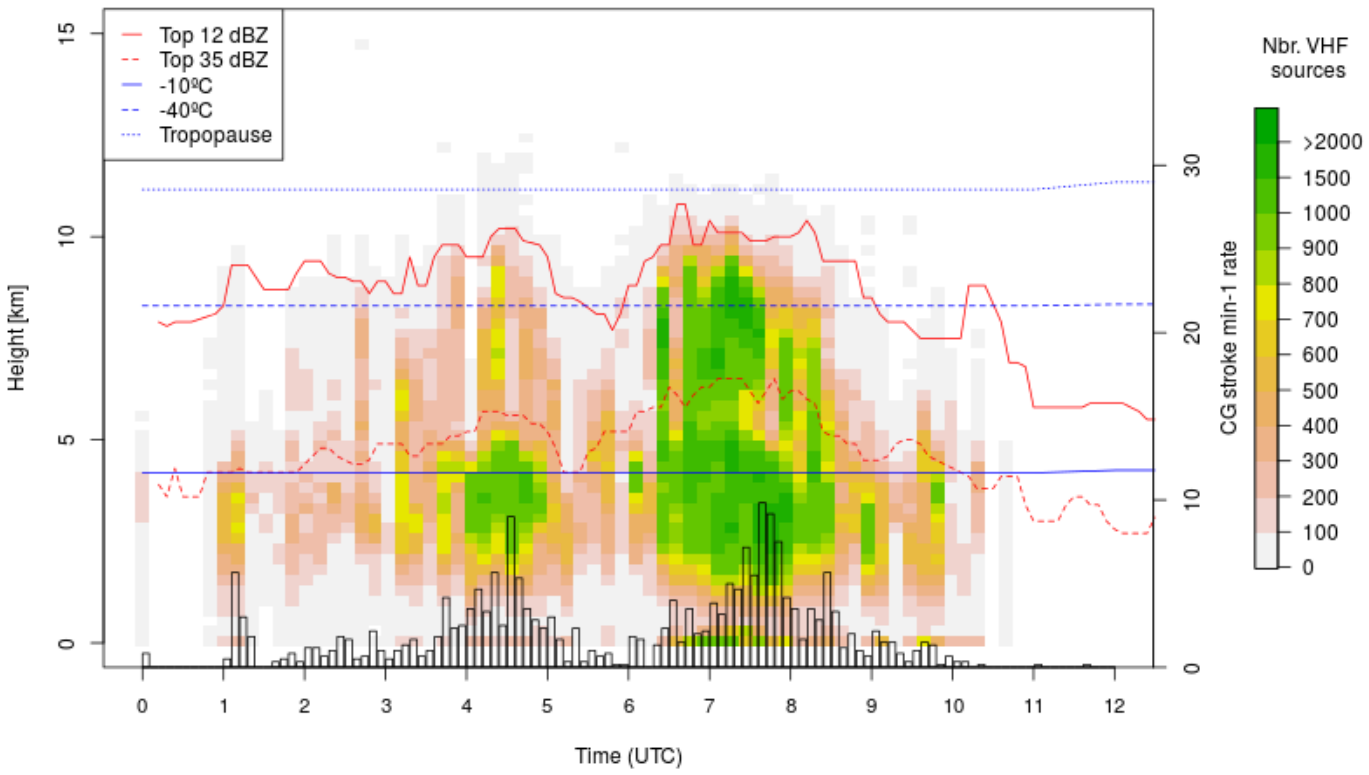

Fig. 4 Analogous to Fig. 2, but showing the evolution on the 20th November 2011. Downward flashes striking WT occurred in two periods, from 04:30 to 04:45 UTC and from 06:55 to 07:15 UTC.

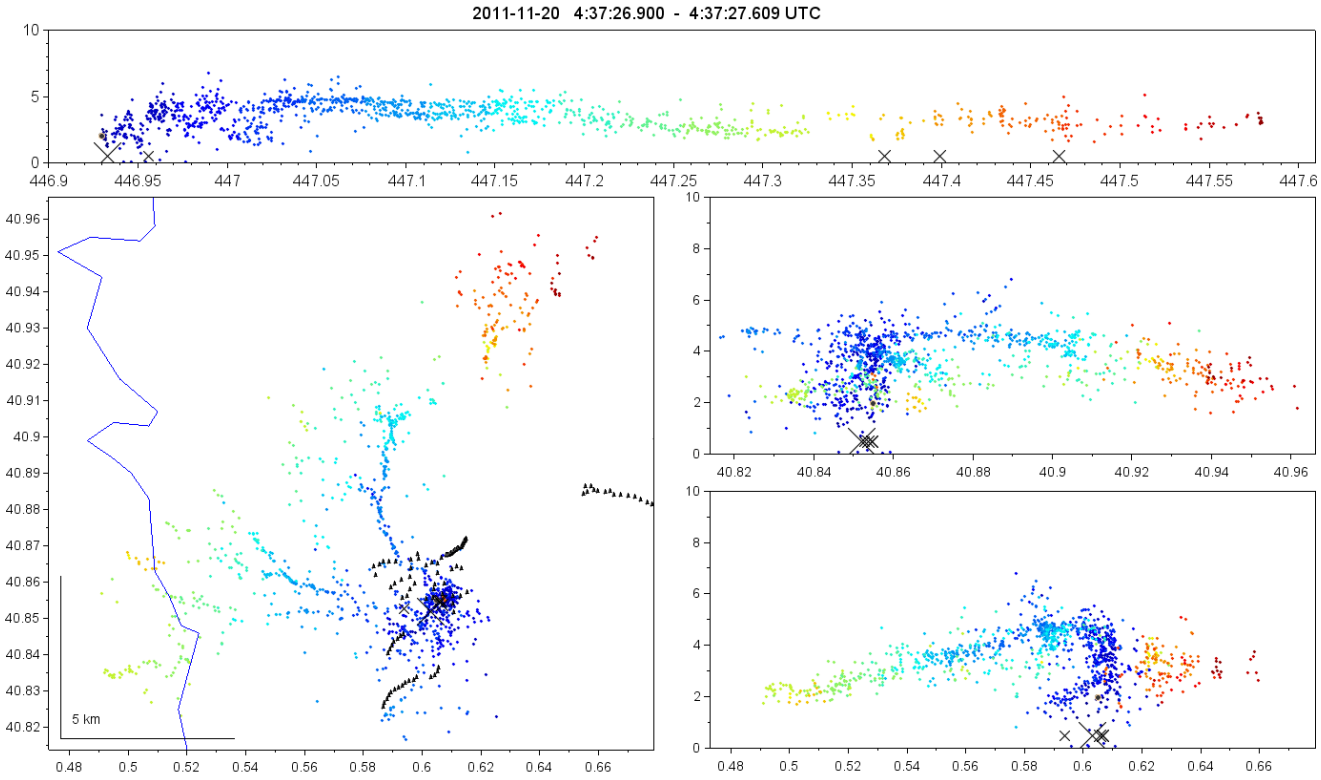

Fig. 5 Multi-panel display of a lightning flash detected by the LMA on the 20th November 2011 at 04:37:26 UTC. VHF sources are coloured as a function of time. The top panel is altitude AMSL (km) versus time (seconds). The left panel is a plan view map (0.1° latitude equals 11.1 km) with contours of the Ebre river (blue) and WT (black triangles) as background. The panels at the right show altitude (km) as a function of latitude and longitude respectively. LINET strokes are displayed with symbols X for negative and + for positive.

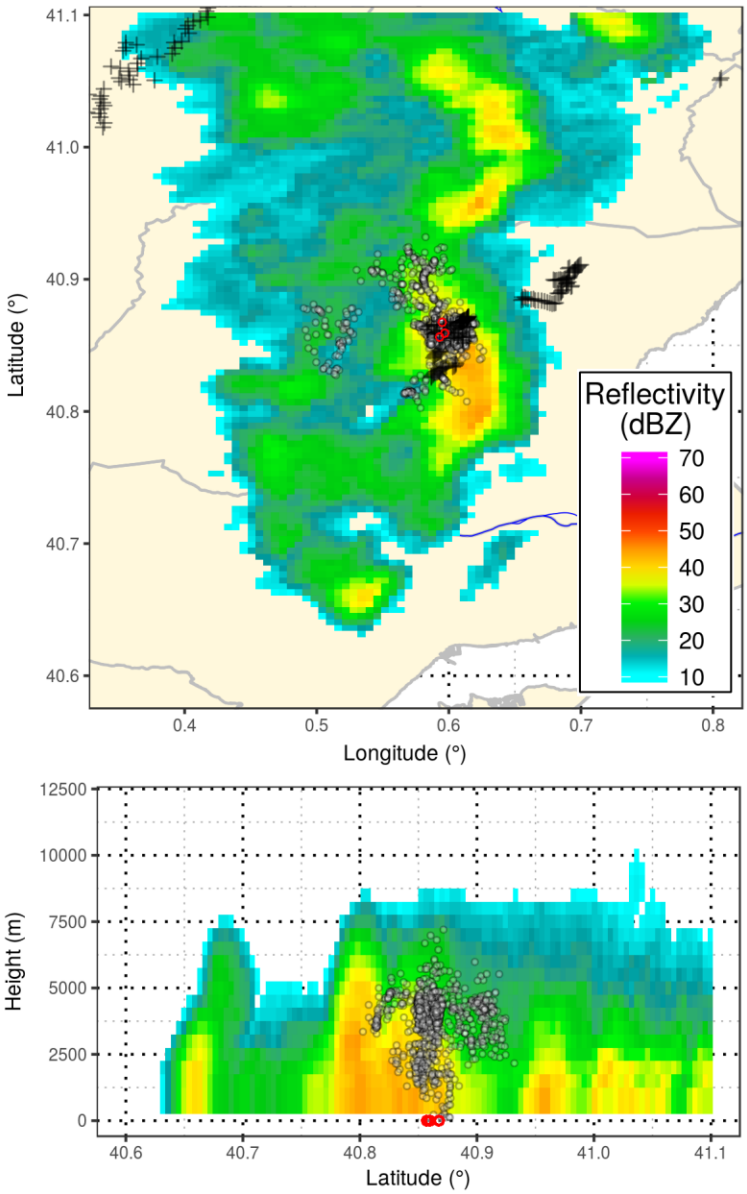

Fig. 6. Radar and LMA lightning data overlay showing the lighting flash to a wind turbine on the 20th November 2011 at 04:39:25 UTC. The LMA sources of a single flash (dots) are combined with the 6–min radar reflectivity volume (04:36-04:42 UTC). LINET CG strokes are represented with red dots. The top panel shows a plain view of the maximum reflectivity (dBZ), while the bottom panel shows the altitude (km) of the LMA sources in the South-North projection of the radar volumetric data. Wind turbines are represented with black crosses.

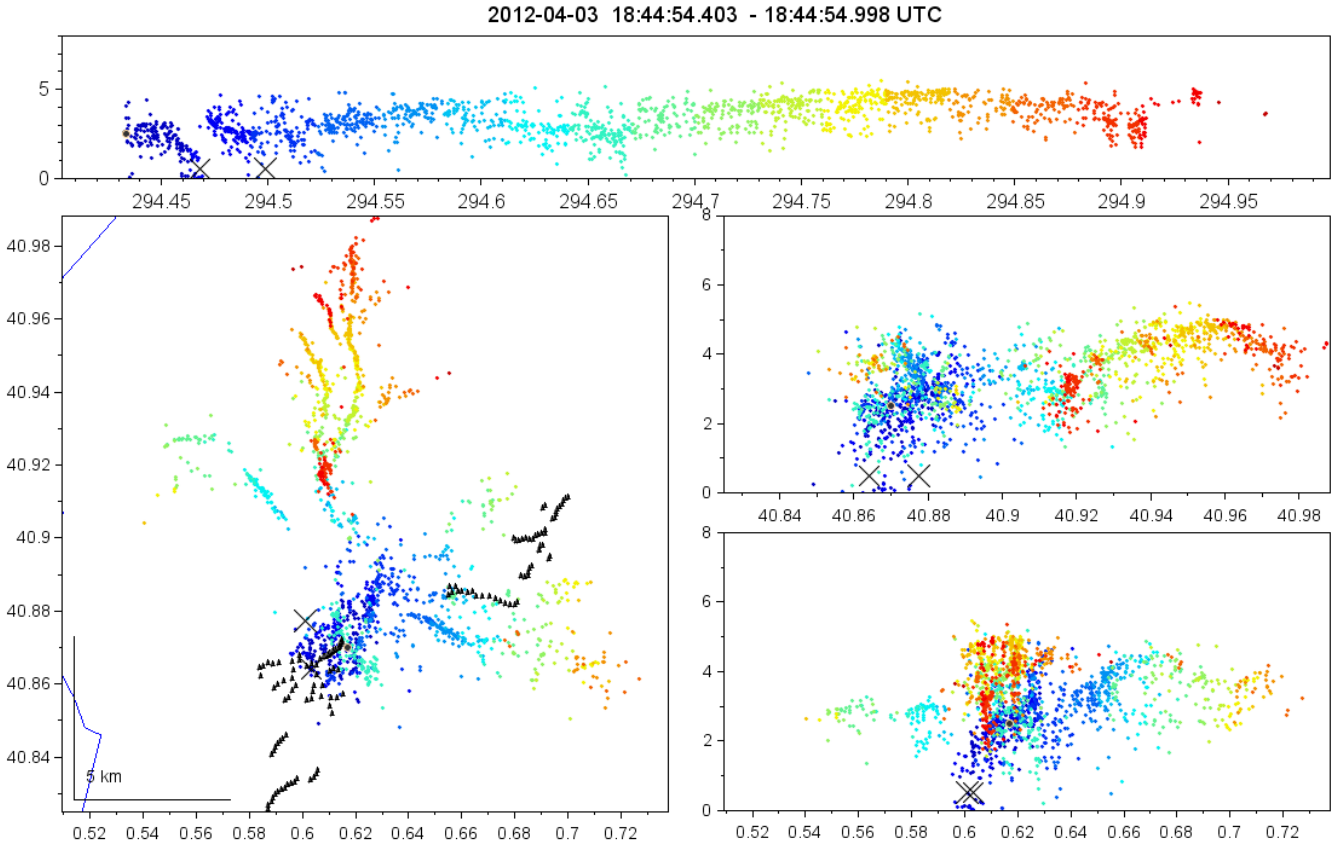

Fig. 7 Analogous to Fig. 5, but for the downward lightning flash to a wind turbine detected by the LMA on the 3rd April 2012 at 184454 UTC.

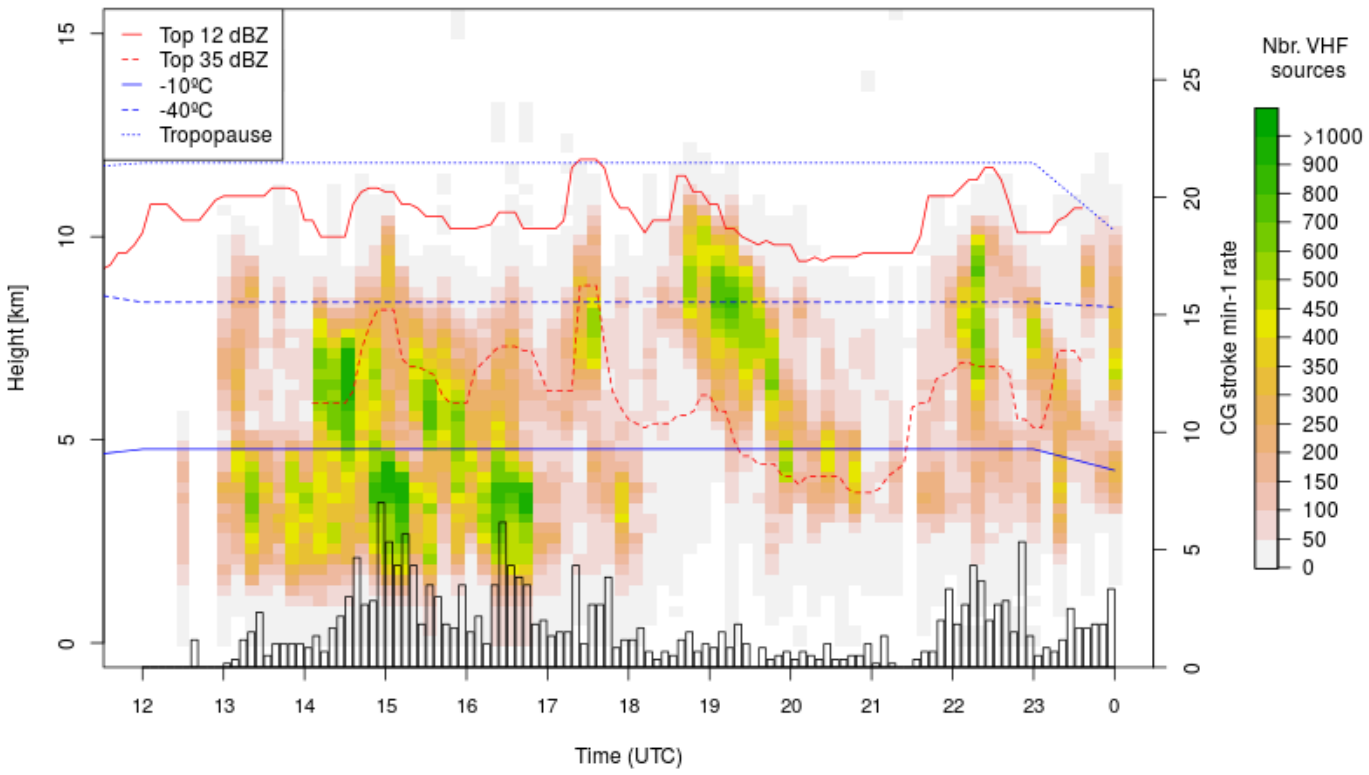

Fig 8. Analogous to Fig. 2, but showing the evolution of the vertical structure of the storms occurring in the area of study on the 17th November 2012

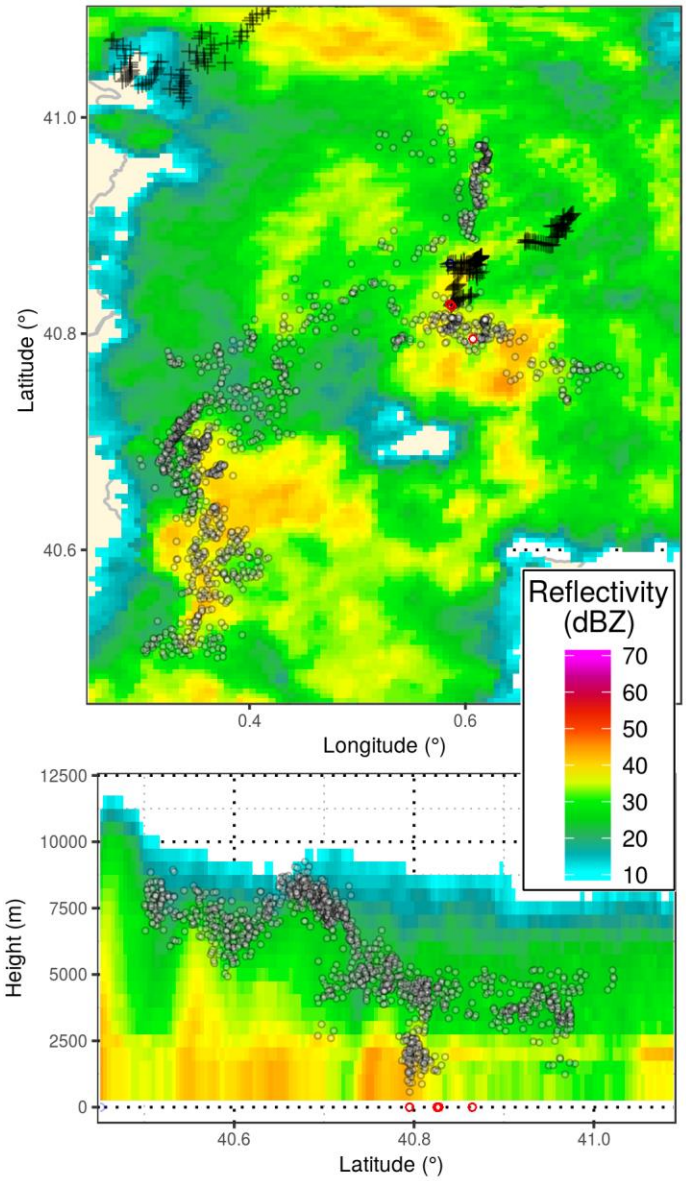

Fig. 9. Analogous to Fig. 6, but showing the 17:34:23 UTC lightning flash to a wind turbine on the 17th November 2012.

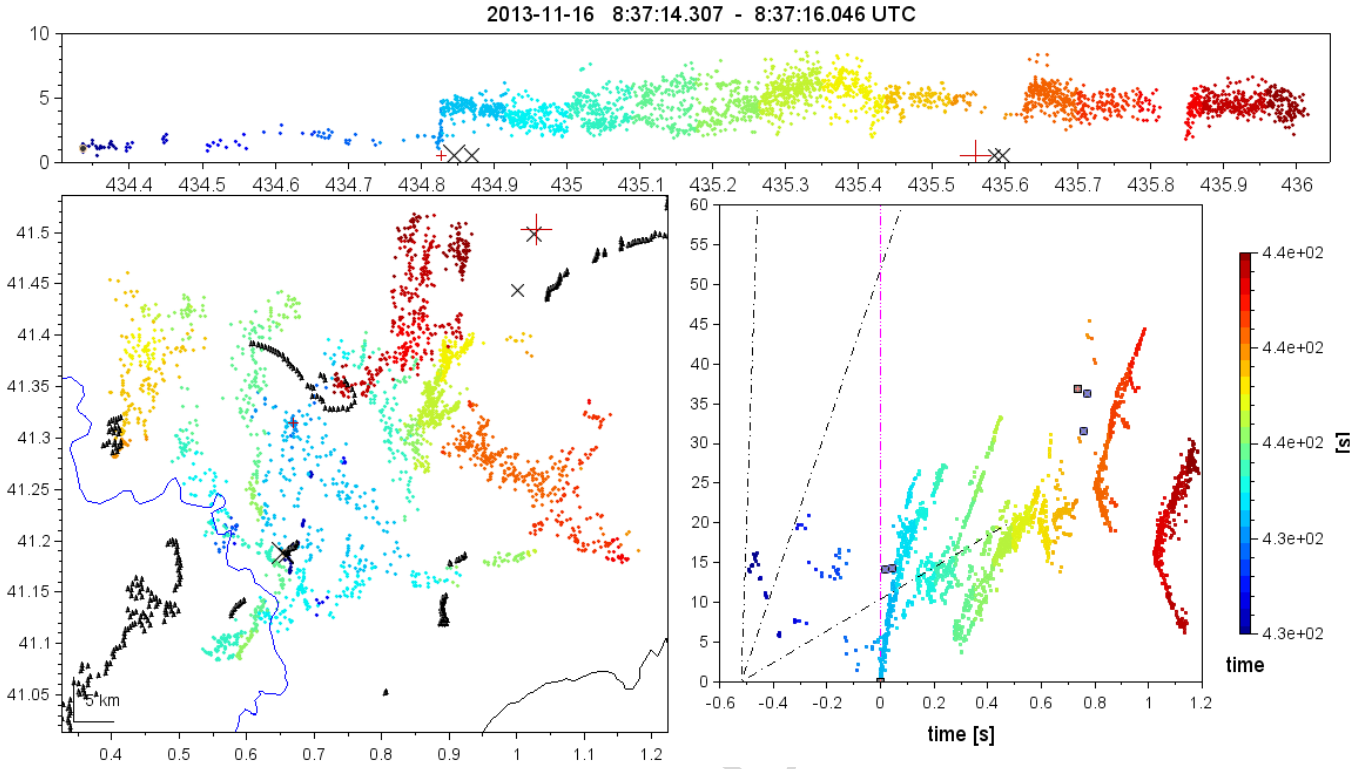

Fig. 10 Multi-panel display of a downward lightning flash to a wind turbine detected by the LMA on the 16th November 2013 at 08:37:14 UTC. For top and left panels see legend in Fig. 5. Unlike the previous LMA figures, here the right panels show the time-distance graph. The dashed reference lines indicate slopes corresponding to speeds of $2 \cdot 10^4$ ms^{-1}, 10^5 ms^{-1}, and 10^6 ms^{-1}. The reference location for the distance is the initiation point of each flash or a cloud-to-ground stroke (at t=0). Black square marks are low-frequency sources detected by LINET (intra-cloud or cloud-to-ground strokes).

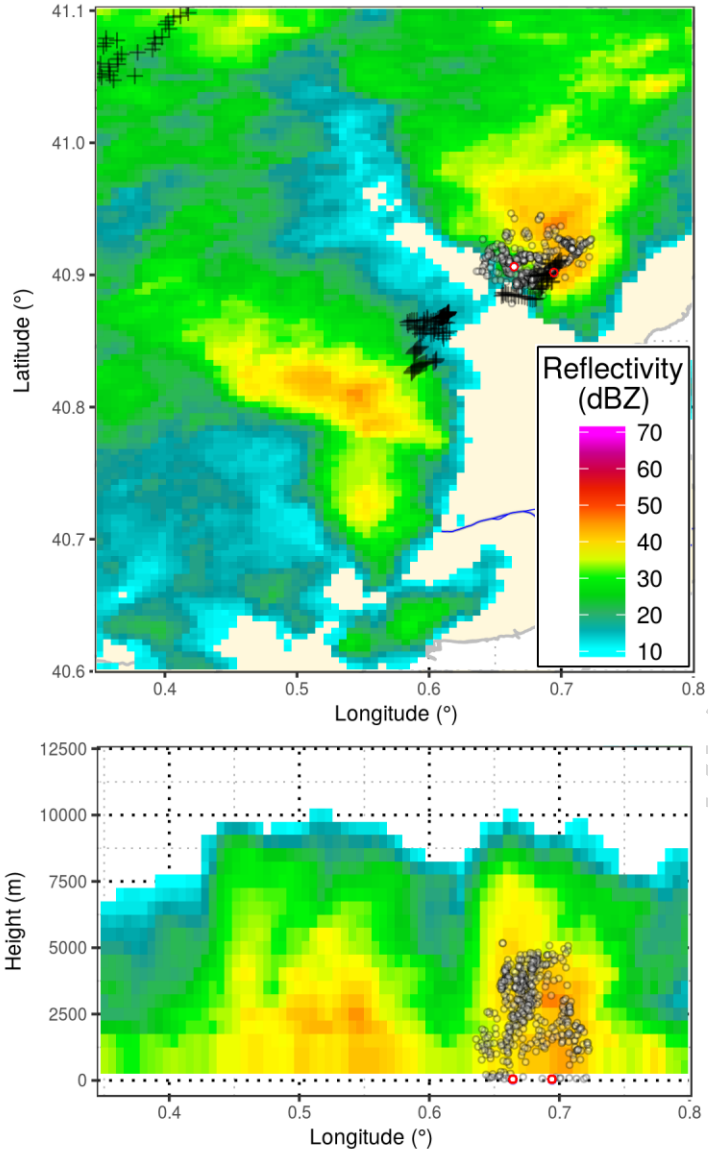

Fig. 11. Analogous to Fig. 6, but showing the 08:40:18 UTC lighting flash to a wind turbine on the 18th January 2014.

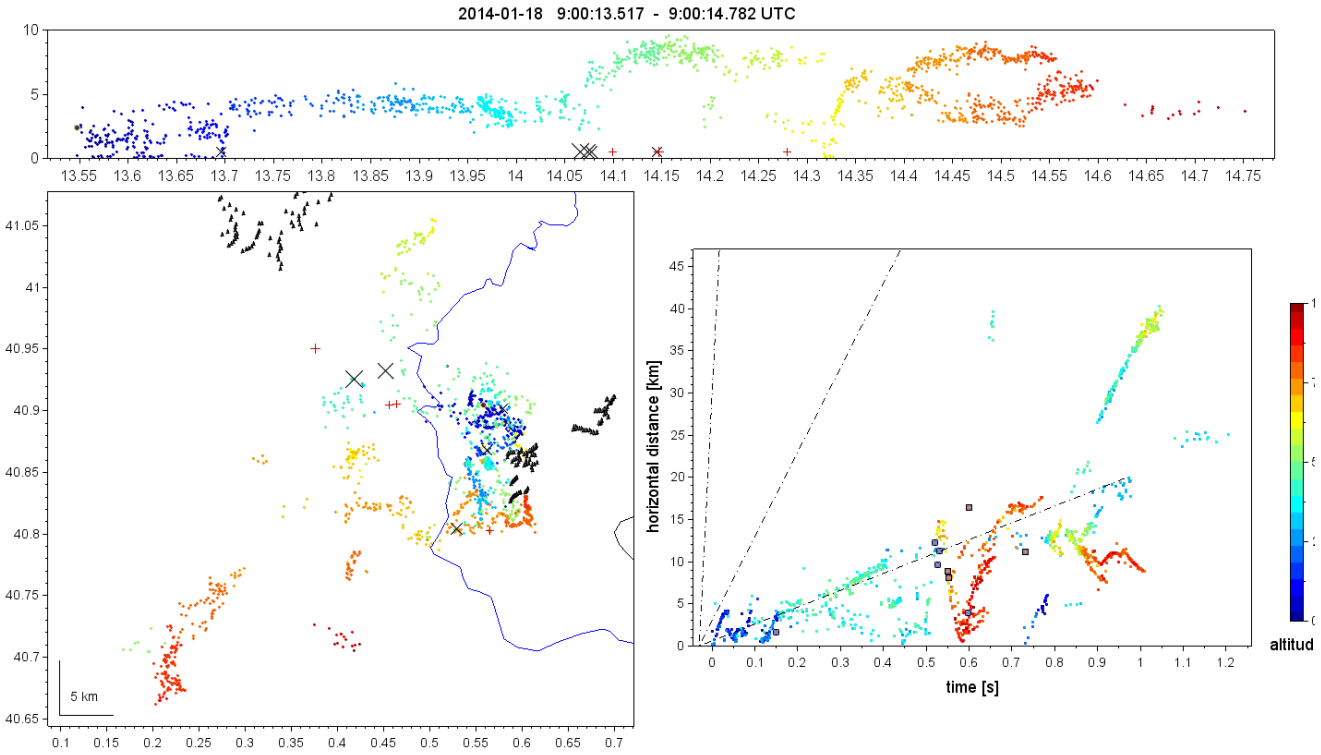

Fig. 12 Analogous to Fig. 10, but for the lightning-triggered upward lightning flash from a wind turbine detected by the LMA on the 18th January 2014 at 09:00:13 UTC.

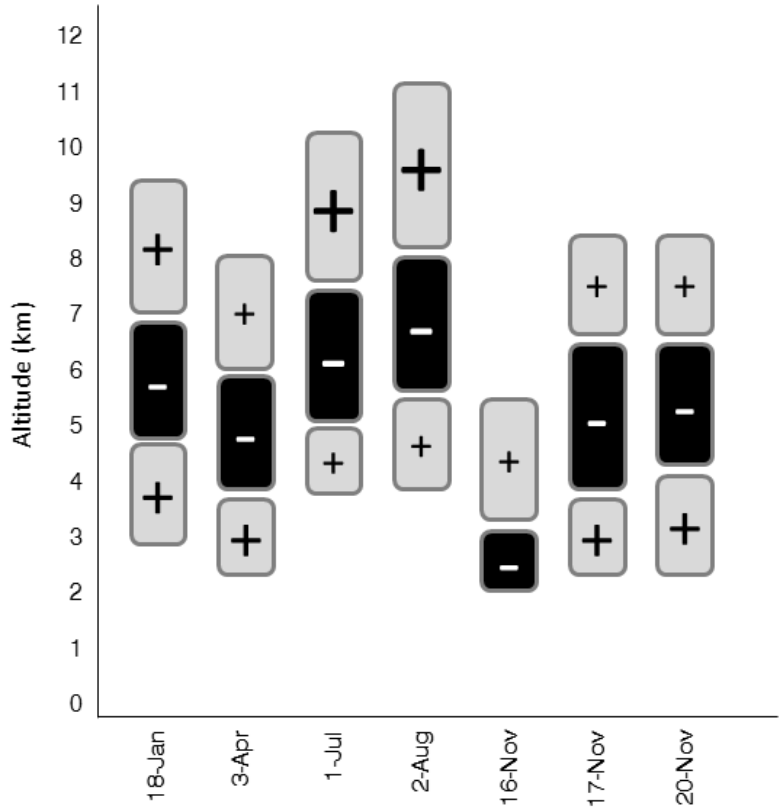

Fig. 13 Charge structure in a vertical profile during the periods for which lightning to/from WT were recorded. The charge structure is inferred from the Lightning Mapping Array (LMA) data analysis, the size of the symbols (+/-) being proportinonal to VHF source density (approximation, not to scale).

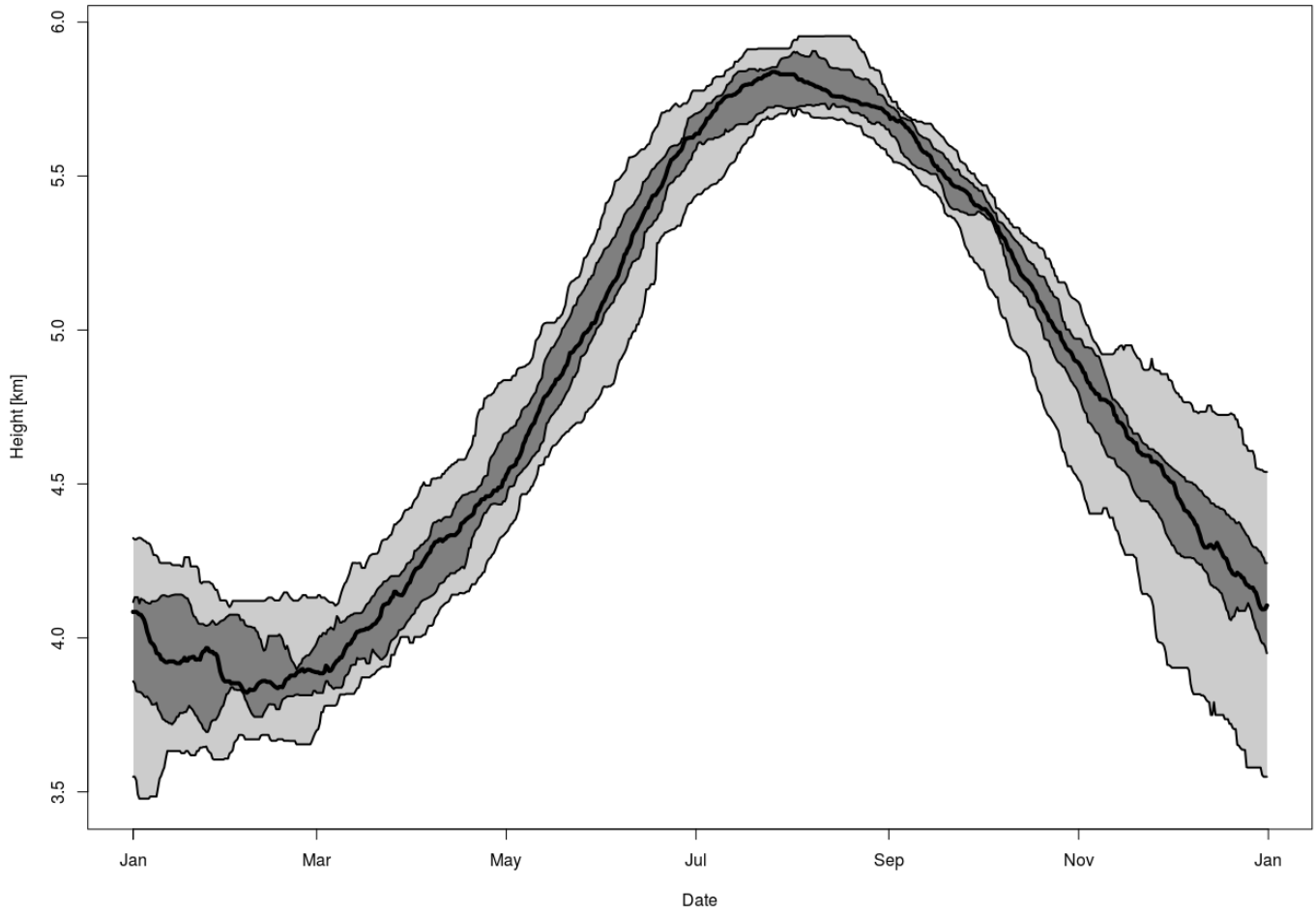

Fig. 14 Annual evolution of the −10°C isotherm height over a 10-year period (2006–2015). Median (bold line), area between percent 25 and 75 (dark grey) and area between min and max (light grey) AMGL Source: Barcelona radiosonde data

HIGHLIGHTS

- Lightning to wind turbines tend to occur outside the main thunderstorm warm-season
- Thunderstorms initiating downwards to wind turbines presented limited vertical developments
- Downwards to wind turbines were mainly negative CGs with peak currents above the average
- Conditions for self-initiated upwards resemble those of Japan /U.S winter thunderstorms